Ternary superhydrides under pressure of Anderson's theorem:

Near-record superconductivity in (La, Sc)H₁₂

Dmitrii V. Semenok^{1, †, *}, Ivan A. Troyan^{2, †}, Di Zhou^{1, †, *}, Andrei V. Sadakov³, Kirill S. Pervakov³, Oleg A. Sobolevskiy³, Anna G. Ivanova², Michele Galasso⁴, Frederico Gil Alabarse⁵, Wuhao Chen^{6,7}, Chuanying Xi⁸, Toni Helm⁹, Sven Luther⁹, Vladimir M. Pudalov^{3,10} and Viktor V. Struzhkin^{11,*}

Abstract

Lanthanum-hydrogen system and its derivatives remain among the most promising for achieving room-temperature superconductivity. In this study, we examined the formation of ternary lanthanum-scandium superhydrides at pressures up to 220 GPa. The primary product of the LaSc alloy's reaction with hydrogen is newly discovered cubic (La,Sc)H₁₂, demonstrating clear superconducting transition in all six channels of the van der Pauw scheme below 244-248 K. In this compound with an unusually large unit cell volume, virtually no magnetoresistance was observed in fields up to 68 Tesla. Synthesized samples of (La,Sc)H₁₂ demonstrate pronounced superconducting diode and SQUID-like effects at a record high temperature of 226 K. Furthermore, our analysis revealed the formation of lower hexagonal polyhydrides (La,Sc)H₆₋₇, which could potentially account for the anomaly in electrical resistance observed near 274 K. This anomalous behavior may be of a superconducting nature, since low-temperature diffraction studies indicate the absence of corresponding structural phase transitions in La-Sc polyhydrides.

1. Introduction

Pressure-stabilized polyhydrides are a new rapidly growing class of high-temperature superconductors 1 , 2 . Remarkable properties of H₃S (critical temperature, T_c = 200 K) 3 , YH₆ (T_c = 224 K) 4 and LaH₁₀ (T_c = 250 K) 5 at 130-200 GPa catalyzed the search for superconductivity (SC) in compressed ternary (X,Y)-H polyhydrides that can be obtained by pulsed laser heating of various alloys and intermetallics with hydrogen or ammonia borane (AB, NH₃BH₃) in diamond anvil cells

¹ Center for High Pressure Science & Technology Advanced Research, Bldg. #8E, ZPark, 10 Xibeiwang East Rd, Haidian District, Beijing, 100193, China

² A.V. Shubnikov Institute of Crystallography of the Kurchatov Complex of Crystallography and Photonics, 59 Leninsky Prospekt, Moscow 119333, Russia

³ V. L. Ginzburg Center for High-Temperature Superconductivity and Quantum Materials, Moscow, 119991 Russia
⁴ Institute of Solld State Physics, University of Latvla, 8 Kengaraga str., LV-1063 Riga, Latvla

⁵ Elettra Sincrotrone Trieste, Strada Statale 14 km163,5 in AREA Science Park, Basovizza, Trieste 34149, Italy ⁶ Department of Physics, Southern University of Science and Technology, Shenzhen 518055, China

⁷ Quantum Science Center of Guangdong-Hong Kong-Macao Greater Bay Area (Guangdong), Shenzhen, China
⁸ Anhui Province Key Laboratory of Condensed Matter Physics at Extreme Conditions, High Magnetic Field
Laboratory of the Chinese Academy of Science, Hefei 230031, Anhui, China.

⁹ Hochfeld-Magnetlabor Dresden (HLD-EMFL) and Würzburg-Dresden Cluster of Excellence, Helmholtz-Zentrum Dresden-Rossendorf (HZDR), Dresden 01328, Germany

¹⁰ National Research University Higher School of Economics, Moscow 101000, Russia

¹¹ Shanghai Key Laboratory of Material Frontiers Research in Extreme Environments (MFree), Shanghai Advanced Research in Physical Sciences (SHARPS), Pudong, Shanghai 201203, China

^{*}Corresponding authors: Dmitrii Semenok (<u>dmitrii.semenok@hpstar.ac.cn</u>), Di Zhou (<u>di.zhou@hpstar.ac.cn</u>) and Viktor Struzhkin (<u>viktor.struzhkin@hpstar.ac.cn</u>).

[†]These authors contributed equally.

(DACs). The uniquely high critical temperatures, upper critical magnetic fields up to 300 T 6 and critical current densities of superhydrides are very attractive for the creation of new electronic devices based on high-pressure DACs. The general and as yet unsolved problem of ternary superhydrides boils down to the question: "Can T_c in ternary polyhydrides be higher than in binary ones and reach room-temperature values?". As the analysis of the thermodynamic stability of the SC state shows, from a fundamental point of view there is no reason why room-temperature superconductivity cannot be achieved in compressed hydrides $^{7-9}$.

Anderson's theorem 10,11 exerts considerable pressure on the experimental search for new high-temperature superconductors in (pseudo)ternary and high-entropy 6 hydride systems, which are perhaps its best illustration 12 . The problem is that the synthesis of hydrides via the laser heating inevitably leads to random mixing of heavy atoms in their sublattice with the formation of solid solutions 13 . A rather long list of already experimentally investigated ternary systems can be given, where the introduction of a third element just slightly changes the critical temperature: $(\text{La,Y})\text{H}_{10}$ 13 , $(\text{La,Y})\text{H}_{4}$ 14 , $(\text{La,Ca})\text{H}_{10}$ 15 , $(\text{Y,S})\text{H}_{9}$ and $(\text{Y,S})\text{H}_{6}$ 16 , $(\text{La,Al})\text{H}_{10}$ 17 , $(\text{La,Be})\text{H}_{8}$ 18 ... Moreover, in the case of introduction of atoms with f-electrons a significant decrease of T_c is observed: $(\text{La,Nd})\text{H}_{10}$ 12 , $(\text{Y,Ce})\text{H}_{x}$ 19 and $(\text{La,Ce})\text{H}_{9-10}$ 20,21 serve as examples. The recent synthesis of the ordered (truly) ternary hydride $\text{LaB}_{2}\text{H}_{8}$ 22 also does not solve the problem, since its T_c is only slightly higher than that of LaH_{4} 20 or $\text{La}_{4}\text{H}_{23}$ 23,24 . A solution may be a "cold" synthesis from H_{2} and intermetallics, in which the heavy atoms remain in their positions and the hydrogen slowly diffuses and dissociates in the metallic sublattice.

In this work, we turn our attention to the La-Sc-H system at pressures up to 230 GPa. In this system a room-temperature superconductivity has recently been predicted for both the binary phase $Pm\overline{3}$ -ScH₁₂ ²⁵, and for the ternary one P6/mmm-LaSc₂H₂₄ ²⁶ (XH₈ type). The experiment indeed shows the formation of a (La,Sc)H₁₂ with T_c = 244-248 K, however, with a different symmetry of the cubic lattice (fcc). Samples of (La,Sc)H₁₂ exhibit a pronounced diode effect and SQUID-like resistance oscillations ²⁷ accompanied by the disappearance of residual resistance below 215 K at all six van der Pauw channels.

2. Results and Discussion

We studied three samples of La-Sc hydrides under pressure: DAC LS-1, DAC LS-2 prepared for low-temperature X-ray diffraction (XRD), and DAC LS-3 designed for pulsed magnetic fields. In all cases, a La-Sc 1:1 alloy, obtained by sintering of La and Sc metal powders in an argon arc, was used. The composition and distribution of elements in the LaSc alloy were confirmed by X-ray fluorescent (XRF) analysis (Figure 2b, Supporting Figures S1-3). Ammonia borane (AB, NH₃BH₃) was used as a source of hydrogen. Laser heating was carried out through a series of \sim 0.3 s infrared laser pulses (λ = 1.06 μ m), in which the sample temperature increased to at least 1000-1500 K leading to the decomposition of AB. In general, the DACs preparation and transport measurements are similar to our previous works ²⁸. A detailed description of high-pressure DACs is given in Supporting Table S1.

2.1 Synthesis of La-Sc polyhydrides at 189-196 GPa

Powder X-ray diffraction (XRD) combined with first-principles calculations of the unit cell volume, thermodynamically stable structures, and electron-phonon mediated superconductivity is the standard method for establishing the structure of superhydrides ^{1,29}.

This led to the choice of XRD as the first step of our research. X-ray diffraction study of a DAC LS-1 sample synthesized at 196 GPa shows the presence of a cubic $(Fm\bar{3}m)$ phase as the main

reaction product (Figure 1a). But what is surprising is the unit cell volume of the resulting compound: almost 32 Å³ per metal atom exceeds the expected volume of the LaH₁₀ at 196 GPa. But given that 50% of the alloy is much smaller Sc atoms, we have to attribute a larger amount of hydrogen to the chemical formula of this compound. It should be (La,Sc)H₁₂. Indeed, fcc-ScH₃ at 140 GPa has a unit cell volume 15.05 Å³/Sc ³⁰, whereas fcc-LaH₃ at the same pressure has the volume of 20.5 Å³/La ⁵. Therefore, difference in the volumes $V(La) - V(Sc) \approx 5.45 \text{ Å}^3$ per atom at 140 GPa. If we take this difference into account and consider a slight decrease in cell volumes during compression to 2 Mbar, the amount of hydrogen in the resulting compound will be equivalent to the same in LaH₁₂ ^{5,31}. This also corresponds to the unusually large unit cell volume of "LaH_{10+δ}" obtained from single-crystal Xray analysis of lanthanum hydrides ³². Moreover, we believe that La superhydride with the canonical formula "LaH₁₀" is rare in experiments. Instead, since the earliest works, it demonstrates variability in composition within the range of XH₉₋₁₂ ³³, at the same maintaining an almost constant maximum critical temperature of about 250 K. This amazing constancy of the maximum T_c , which does not depend on randomly distributed impurities (B, N, Al, Ca, Y, Sc ...), nor on the method of obtaining La superhydride, nor on variations in the composition of hydrogen (± 1 -2 H atoms), is, in our opinion, one of the most striking manifestations of Anderson's theorem ¹⁰.

Due to the absence of additional X-ray reflections from the scandium sublattice, we will further consider the (La,Sc) solid solution model for the heavy atom sublattice. This situation is common for many ternary polyhydrides 12,13,15,20,21 . There is no doubt that several other phases are present in the sample, as the number of peaks exceeds that for both the $Fm\overline{3}m$ -(La,Sc)H₁₂, as well as the number of reflections for a distorted phase F(P)mmm-(La,Sc)H₁₂ (see Supporting Figure S4). The latter one is likely formed due to the large difference in volumes and properties of La and Sc atoms. Existence of side phases in the sample also follows from the presence of several steps in the observed SC transitions (Figures 3,4). Additional XRD reflections may appear from Ta/Au electrodes and from the lower hydride $Fm\overline{3}m$ -(La,Sc)H₂ (Figure 1c).

The X-ray diffraction study of the sample in the DAC LS-3 at 189 GPa was limited by the small diameter (d = 15.3 mm) of this asymmetric cell intended for studies in pulsed magnetic fields. The result of the XRD measurements was quite unexpected: instead of the usual $Fm\overline{3}m$ -like pattern we discovered a hexagonal pattern that can be refined as P6/mmm (Figure 1e). Recently, a similar structure, P6/mmm-LaSc₂H₂₄ (XH₈ type), was predicted to be a room-temperature superconductor with $T_c = 316$ K below 200 GPa ²⁶. This compound has a calculated unit cell volume of 24.15 Å³/(La, Sc) at 200 GPa ²⁶ which is significantly less than the expected volume of LaH₈ due to the smaller volume of the Sc atom. The experimental cell volume of the phase (La,Sc)H_x that we obtained in DAC LS-3 is 22.4 Å³/(La, Sc) at 189 GPa despite the higher content of La. This indicates that the hydrogen content is less than in the predicted LaSc₂H₂₄ and its chemical formula is (La,Sc)H₆₋₇. As we will see below, presence of this hexagonal phase in DAC LS-3 may be reflected in the temperature dependence of the electrical resistance, demonstrating a pronounced drop at ≈ 274 K, noticeably higher than T_c of cubic (La,Sc)H₁₂ (Figures 3, 4a).

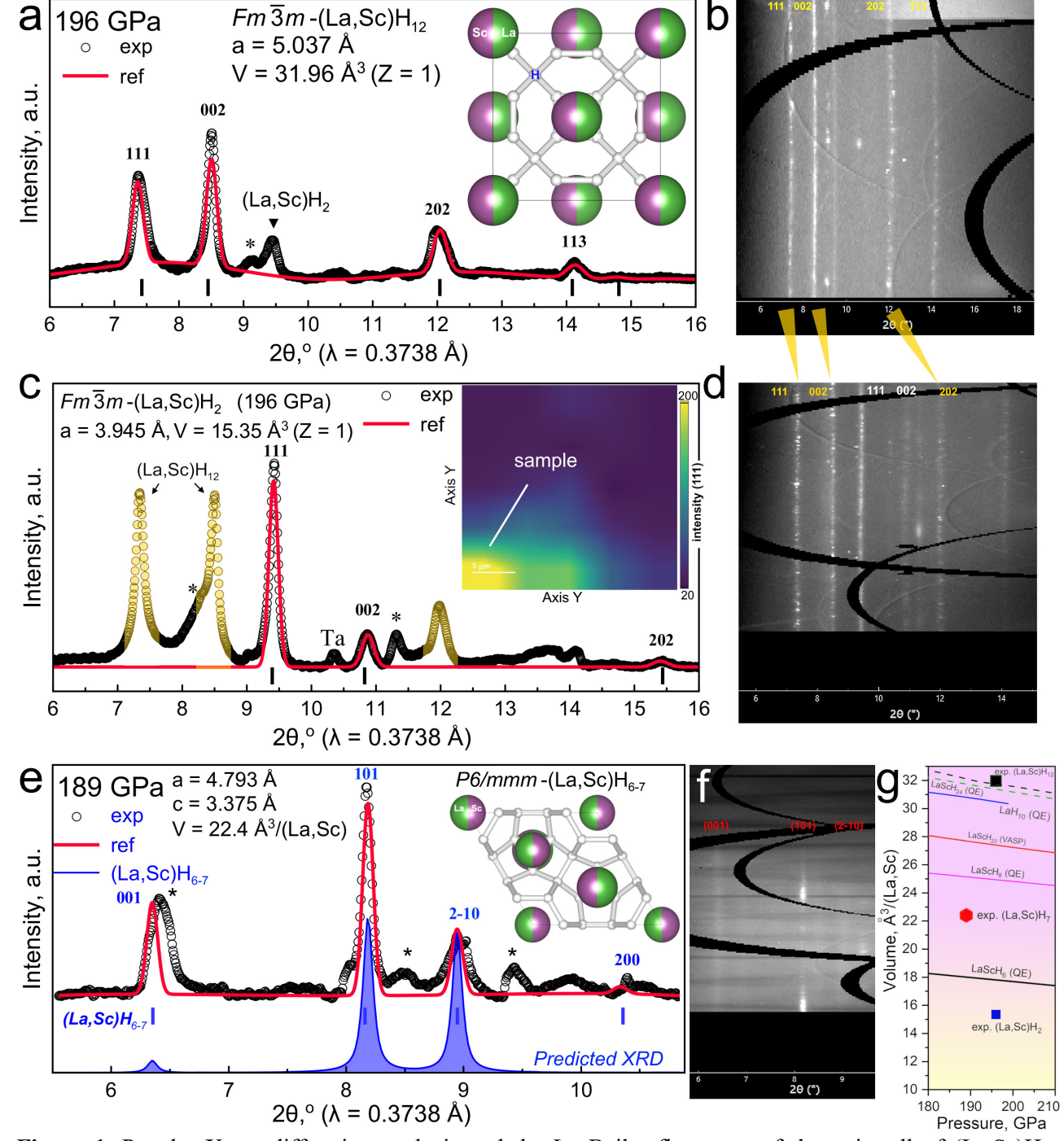


Figure 1. Powder X-ray diffraction analysis and the Le Bail refinements of the unit cell of (La,Sc)H₁₂, (La,Sc)H₇ and (La,Sc)H₂ phases in DACs LS-1 and LS-3 at 189-196 GPa. (a) Le Bail refinement of the unit cell parameters of Fm3m-(La,Sc)H₁₂ (JANA2006) in DAC LS-1: black points mark experimental data, the red line – is the refinement. Inset: structural model of this compound based on a cubic La sublattice of LaH₁₀. Asterisks mark unexplained reflections. (b) X-ray diffraction image ("cake") of the sample in DAC LS-1. (c) Experimental XRD and Le Bail refinement of the unit cell parameters of Fm3m-(La,Sc)H₂ (JANA2006). Yellow color marks reflections from Fm3m-(La,Sc)H₁₂. "Ta" indicates to a possible peak from Ta/Au electrodes. The inset shows spatial distribution of (La,Sc)H₁₂ 111 reflection. (d) Typical X-ray diffraction image ("cake") which contains reflections from both (La,Sc)H₂ and (La,Sc)H₁₂. (e) Experimental XRD pattern and Le Bail refinement of the unit cell parameters of (La,Sc)H₆₋₇ found in DAC LS-3. Filled blue plot – is calculated XRD pattern for predicted P6/mmm-LaSc₂H₂₄ with solid solution of (La, Sc) in metal sublattice. (f) X-ray diffraction image ("cake") of the sample in DAC LS-3. (g) Calculated equations of state (QE, VASP codes) and experimental unit cell volumes used to estimate the H-content in obtained compounds.

In 2020-2021, it was suggested that compressed hydrides may not be superconductors, and resistive transitions in them are a consequence of structural phase transitions ³⁴. This was facilitated by the absence of X-ray diffraction data near observed transition temperatures. The lack of structural information motivated our low-temperature X-ray diffraction experiment with (La,Sc) hydrides at 150 GPa performed at the Xpress beamline of the Elettra synchrotron radiation facility. Gold piece was used as the pressure gauge in these experiments.

In this part of the work, we synthesized La-Sc ternary hydrides at 150-153 GPa (Figure 2a) in DAC LS-2 from the corresponding 1:1 La-Sc alloy, the X-ray fluorescence (XRF) analysis of which is shown in Figure 2b. The main product of the reaction at this pressure can be refined using hexagonal systems, for example, $P6_3/mmc$ -ScH₆, predicted by Hou et al. ³⁵ However, the ratio c/a = 1.26 is unusual for this space group (Figure 2c). The unit cell volume of obtained compound is 21.85 Å³/(La, Sc) which indicates composition of (La, Sc)H_{6-x} similar to the predicted hexagonal ScH₆ ³⁵. We believe that the proposed $P6_3/mmc$ structure describes well the resulting diffraction pattern except for an unexpectedly low intensity of the (101) reflection (Figure 2b), and can serve as a first approximation for further structural analysis. Comparison of the experimental unit cell volume, 21.85 Å³/(La, Sc), with the theoretical calculation (V_{DFT} = 23.64 Å³/(La, Sc)) shows that the hydrogen content in this hexagonal phase is between 5 and 6 per metal atom. It should be noted, that the intensity of the XRD pattern in low-temperature cryostat appears insufficient to accurately refine the unit cell parameters at all studied pressure points (Supporting Table S2).

The DAC was cooled to a temperature of 150 K while low-temperature powder XRD was recorded. No obvious phase transitions were observed between 150-300 K and 153-169 GPa (Figure 2e). However, there are some signs of small distortion of the crystal lattice at 200-250 K: splitting of the (100) reflection and anomaly of the *c/a* ratio (Figure 2e, Supporting Table S2). When cooled to 100 K, the pressure in DAC LS-2 increased so much that caused collapse of diamond anvils followed by the pressure drop to 30 GPa. The XRD pattern obtained at 30 GPa and 300 K indicates a significant change in the structure and H-content of the (La,Sc) hydrides, and can be described as a two-phase sample consisting of tetragonal *I4/mmm*-(La,Sc)H_{3-x} (phase I) and thermodynamically stable, pseudocubic *P4*₁-(La,Sc)H_{~3} (phase II, Supporting Tables S1 and S6). The deviation from the calculated unit cell volumes of (La,Sc)H_{3-x} and (La,Sc)H₃ indicates the non-stoichiometric composition of the obtained compounds. Moreover, pseudocubic (La,Sc)H₃ probably undergoes tetragonal distortion.

Therefore, surprisingly, the X-ray diffraction study of the La-Sc-H system shows the presence of polyhydrides which are very similar to the predicted ones: these are hexagonal LaSc₂H₂₄ 26 , ScH₆ 35 , and cubic ScH₁₂ 25 . Indeed, in the experiment we see the cubic phase (La,Sc)H₁₂, the hexagonal phases (La,Sc)H_{7-x} and (La,Sc)H_{6-x} at 150 GPa. It was already noticed (for instance, in Refs. 28,36) that structural search programs such as USPEX $^{37-39}$, CALYPSO 40,41 , AIRSS 42,43 are good at calculating the hydrogen content of stable polyhydrides, whereas predicting of correct crystal symmetry is much more difficult. Despite this, first-principles methods provide important clues to the interpretation of products of high-pressure synthesis. In our experiment we see La-Sc hydrides with the predicted stoichiometry, but with a different lattice symmetry.

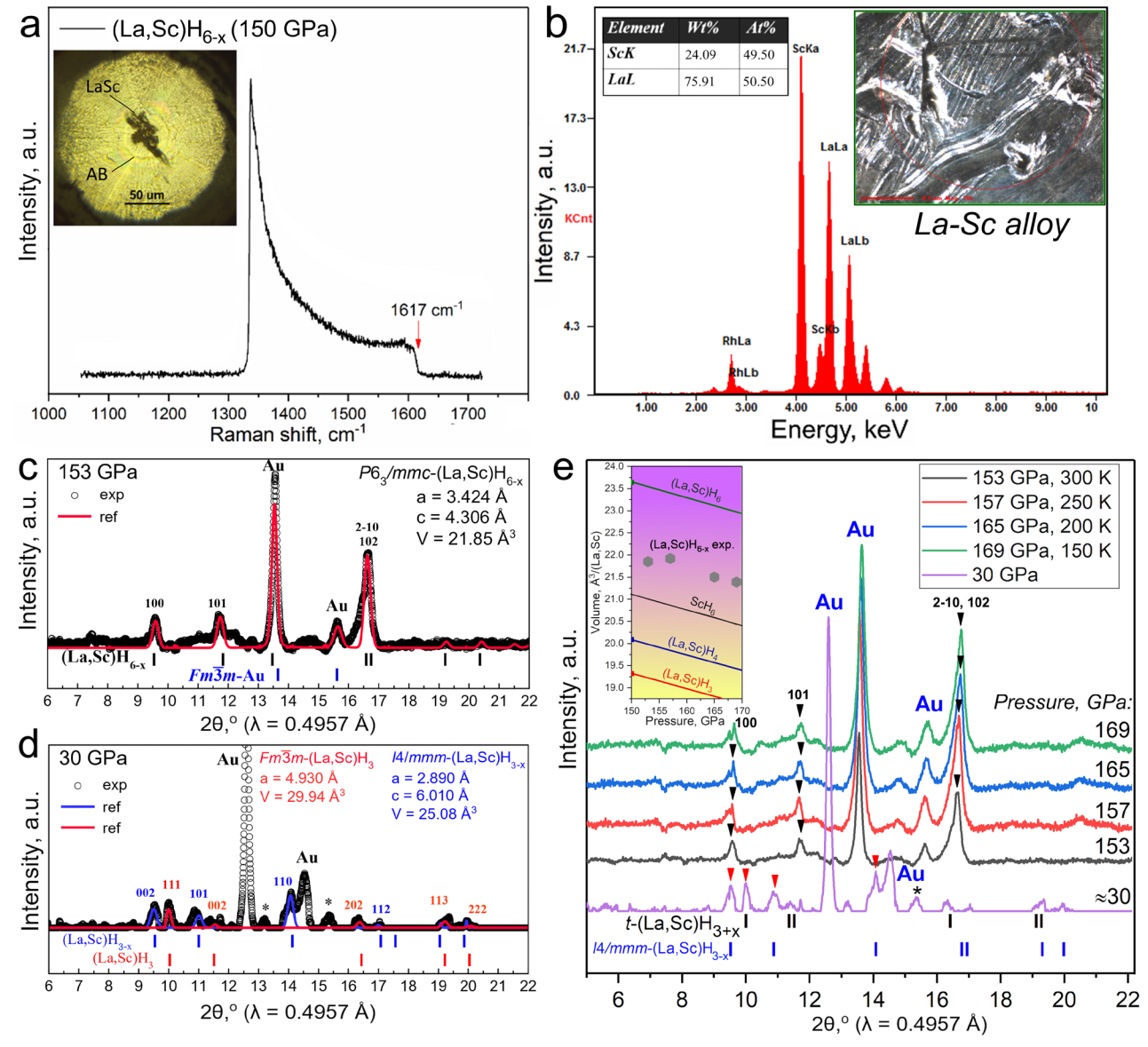


Figure 2. Synthesis and X-ray diffraction of La-Sc hydrides in DAC LS-2 at 150-153 GPa. (a) Raman spectrum of the sample in DAC LS-2 in the region of C-C vibrations after laser heating. Inset: photo of the sample. (b) X-ray fluorescence analysis of initial La-Sc alloy. Composition is close to 1:1 (see Table in the inset). (c) Experimental X-ray diffraction patterns and Le Bail refinements of unit cell parameters of hexagonal (La,Sc)H_{6-x} at 153 GPa (300 K). "Au" - denotes reflections from gold used as the internal pressure sensor. Asterisks indicate uninterpreted peaks. (d) The same for tetragonal (La, Sc)H_{3-x} and pseudocubic (La, Sc)H₃ at 30 GPa after collapse of the DAC LS-2. (e) A series of XRD patterns of the DAC LS-2 sample taken during decreasing temperature from 300 to 150 K with a step of 50 K. As it cooled, the pressure in the DAC spontaneously increases with $dP/dT \approx -0.11$ GPa/K. The pattern at 30 GPa corresponds to a broken DAC.

2.3 Superconductivity of La-Sc polyhydrides

Transport properties of La-Sc hydrides at 196 GPa were studied in high-pressure DACs LS-1 and LS-3. We used diamond anvils with a culet diameter of 50 μ m, equipped with four sputtered (Ta/Au) electrodes and tungsten gasket covered by CaF₂/epoxy insulating layer. For a detailed description of the experiment, see Supporting Information. The studies were performed in both direct current (DC, Figure 3a), and alternating current (AC) modes. Regardless of the test method chosen, (La,Sc)H₁₂ sample in DAC LS-1 shows a disappearance of electrical resistance below 235 K (Figure 3a). Transport measurements (Figures 3a, d) indicate the possible presence of two phases in the sample, with close critical temperatures: T_c (onset) \approx 247-248 and 242 K. The broadening of superconducting transitions in a magnetic field is insignificant, as for many other polyhydrides ⁴⁴

which is associated with a high concentration of defects, pinning centers and very high depinning potential barriers reaching in hydrides $1-2\times10^5$ K 45,46 . This correlates with virtually zero magnetoresistance (MR) over the studied range of temperatures (170-223 K) and magnetic fields (Figure 3e).

In some cases, non-uniform distribution of sample conductivity in the van der Pauw circuit leads to "false" voltage (resistance) drops, which actually correspond to a local increase in the resistivity ³⁴. Such voltage drops may be incorrectly interpreted as superconducting transitions. In this situation, it is necessary to examine all combinations of electrodes. For a four-electrode circuit there are six different channels, two of them are "diagonal" (or the Hall type). Results of measuring the voltage drop across the (La,Sc)H₁₂ sample at 196 GPa on four off-diagonal electrode combinations vdp1-4 are presented in Figures 3a-b. In the region of the SC transition, the resistance decreases from $\approx 0.1 \Omega$ to 1-2 $\mu\Omega$, that is, by a factor of 10⁵. The thermal noise of the measuring circuit is symmetrical on all four channels. Moreover, the diagonal channels (*diag1,3* and *diag2,4*, see Supporting Figure S8) also show the disappearance of the sample's electrical resistance and symmetrical residual thermal noise. The obtained result excludes the possibility of any metal-insulator transitions in the sample.

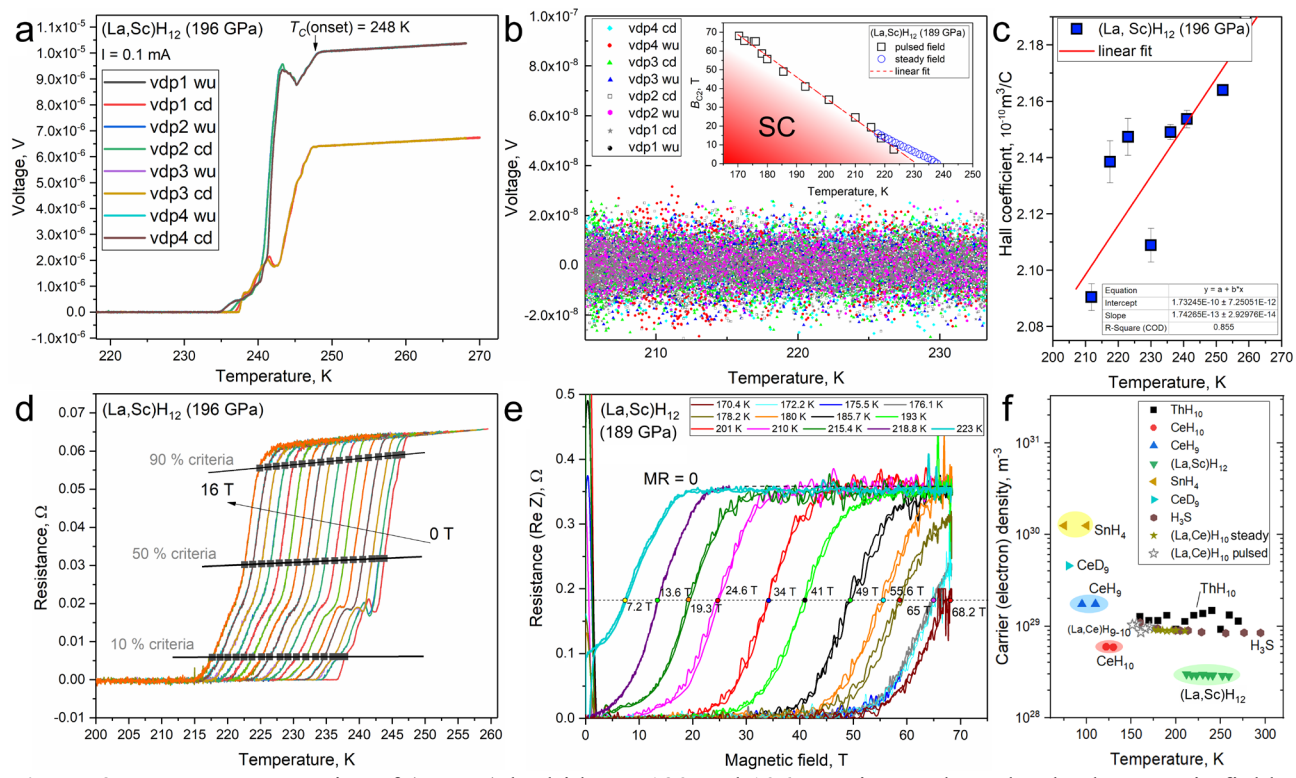


Figure 3. Transport properties of (La, Sc) hydrides at 189 and 196 GPa in steady and pulsed magnetic fields. (a) Dependence of the voltage drop across the DAC LS-1 sample (La, Sc)H₁₂ on temperature in the warming ("wu") and cooling ("cd") cycles for four direct channels of the van der Pauw circuit (vdp1-4). Here we used the delta mode with a DC excitation current of 0.1 mA. (b) Residual voltage on the sample after transition to the superconducting state on four direct channels (vdp1-4) in the cooling and warming cycles. Average residual resistance of the sample is ~1-2 μΩ. Inset: the boundary of the SC and non-SC regions on the phase diagram, as well as the $B_{C2}(T)$ temperature dependence in magnetic fields up to 68 T, the R_{50%} criterion was applied. (c) Temperature dependence of the absolute value of Hall coefficient in (La, Sc)H₁₂ at 196 GPa. Steady fields ± 33 T were used for measurements. Red line – is the linear fit. (d) Temperature dependence of the electrical resistance of the (La, Sc)H₁₂ in various constant magnetic fields from 0 to 16 Tesla. The criteria $R_{10\%}$, $R_{50\%}$, $R_{90\%}$ were applied to determine $B_{C2}(T)$. (e) Dependence of the real component of the electrical resistance of the sample in DAC LS-3 on a pulsed magnetic field up to 68 T at various temperatures from 223 K to 170.4 K. "MR" denotes magnetoresistance. (f) Carrier (electron) concentration in various superhydrides according to the Hall coefficient measurements: $n_e = 1/eR_H$. Thickness of all samples is assumed 1 μm.

We studied the behavior of La-Sc hydrides in steady (0 - 33 T, DAC LS-1) and pulsed magnetic fields with a pulse duration of 150 ms and maximum field induction of 68 T (DAC LS-3).

Since the primary superconducting transition in DAC LS-3 sample is observed at the $T_c \approx 244$ K (Figure 4a), we will henceforth consider (La,Sc)H₁₂ to be the main content of the LS-3 sample. Such a strong pulsed magnetic field was used to establish the shape of the superconducting phase diagram (inset in Figure 3b). In this case, measurements of the dependence of the electrical resistance (real part, Re Z) on the magnetic field were carried out in AC mode at frequencies of 16.66 kHz and 33.33 kHz in the temperature range from 170.4 K to 223 K (inset in Figure 3e). In this range of temperatures and fields, the magnetic phase diagram of (La,Sc)H₁₂ is linear ($dB_{C2}/dT \approx 1.15$ T/K), as for many other hydrides ^{12,47,48,49}. Very high upper critical field $B_{C2}(0)$ of La-Sc superhydrides is remarkable. The extrapolated value of $B_{C2}(0)$ can exceed 200-230 T (Figure 3b). Such high upper critical field is characteristic of dirty ("hard") superconductors and high-entropy polyhydrides ⁶.

Metal superhydrides synthesized at high pressure are, in most cases, fine powders ⁵⁰ with a large number of defects in microcrystals ^{1,12,28,51}. This determines many physical properties of hydrides. For example, wide diffusive XRD patterns ^{36,52,53}, very low RRR (residual-resistance ratio) about 1.1–1.5 ⁴, and often near zero magnetoresistance. Typically, the magnetoresistance of metals is positive and $\propto \mu_e^2 B^2$, where μ_e is the electron mobility (in the absence of holes). However, hydrides are different. The existence of a region of negative magnetoresistance was established in La₄H₂₃ ^{23,24} and CeH₁₀ ⁵⁴, whereas magnetoresistance of (La,Sc)H₁₂ in DAC LS-3 is practically equal to zero like in graphene ⁵⁵. It may be an evidence of non-Fermi-liquid behavior of the La-Sc hydrides, as we previously found in our studies of (La,Nd)H₁₀ ¹² and SnH₄ ²⁸.

One of the most likely explanations of this fact is a very defective and finely dispersed structure of the sample containing B, N impurities from ammonia borane, fluctuations of Sc and La concentration like in NbTi 56 , presence of H₂ molecules and H vacancies. In this case, the electron free path (l_e) is significantly less than the Larmor radius (r_g) even at 70 T

$$l_e \ll r_g = \frac{m_e^* v_F}{eB},\tag{1}$$

where the Fermi velocity v_F can be estimated as $\sim 3 \times 10^5$ m/s ⁵⁷, and m_e^* is the effective electron mass. If we take $m_e^* = m_e$ and magnetic field induction B = 50 T, then $r_g \sim 38$ nm. This value should be comparable to the crystallite size and the average distance between defects in (La, Sc)H₁₂. In this case, scattering on defects and grain boundaries will be the dominant process, and the influence of the magnetic field will be insignificant. Of course, it cannot be completely ruled out that the positive magnetoresistance ($\propto \mu_e^2 B^2$), observed due to the distortion of electron trajectories in a magnetic field, can compensate for negative magnetoresistance related to the preformation of Cooper pairs, giving an ultimately zero result in a certain range of magnetic fields.

Finally, we have studied the Hall effect and its sign in the non-superconducting state of (La, Sc)H₁₂ in DAC LS-1. In the Hall measurement scheme, the superconducting transition begins at the same T_c around 245 K, but is accompanied by a more complex behavior of the electrical resistance R(T, B). Supporting Figures S9-11 show that the Hall voltage depends on magnetic field linearly. The Hall coefficient R_H is found negative. This indicates that electrons are the primary charge carriers. $|R_H| = (2.13\pm0.03)\times10^{-10} \text{ m}^3/\text{C}$ in (La, Sc)H₁₂ slightly decreases along with temperature (Figure 3c). This corresponds to increase of carrier concentration by 3 % during cooling from 259 to 212 K: $n_e((\text{La,Sc})H_{12}) = 1/eR_H = (2.95 \pm 0.05)\times10^{28} \text{ m}^{-3}$ (Figure 3f). In general, almost temperature independent carrier concentration is typical for metals. The found values of electron concentration $n_e((\text{La,Sc})H_{12})$, within the accuracy of the error in determining the sample thickness, correspond to the concentration of carriers in other superhydrides (Figure 3f).

When studying the Hall effect in the DAC LS-3, we unexpectedly found that the onset of the resistance drop at a certain stage of the experiment shifted to higher temperatures, reaching unusually high value of 274 K (Figure 4a, Supporting Figures S21). At the same time, the main superconducting transition, probably corresponding to the (La, Sc)H₁₂, was still observed at $T_c = 244$ K. High-temperature superconductivity with $T_c > 270$ K was predicted in both cubic ScH₁₂ ²⁵ and hexagonal LaSc₂H₂₄ ²⁶. Moreover, detected resistance anomaly at 274 K correlates with the presence of a similar hexagonal phase in DAC LS-2 (Figure 1e). Unfortunately, after 8 cooling/heating cycles (Supporting Figure S21), this "metastable" anomaly almost disappeared. However, some residual traces of it in the Hall measurements were found even a month after the initial detection (Supporting Figure S22).

Synthesized samples of La-Sc hydrides are heterogeneous. Trapping of magnetic flux by inhomogeneities in a superconducting sample ⁴⁸ may lead to appearance of SQUID (superconducting quantum interference device) ²⁷ and asymmetric conductivity effects ⁵⁸ in hydrides. The later one, also known as diode effect, can be detected in (La,Sc)H₁₂ superhydride (DAC LS-1) with the help of DC/AC current containing an offset DC current of \pm 1 mA and small sinusoidal signal of 0.1 mA (RMS) with a frequency of 100 Hz ($I(t) = \pm 1 + 0.1 \times \sqrt{2} \sin(100 \times t/2\pi)$ mA, where t is the time). The signal amplitude at the second pair of electrodes of the 4-contact van der Pauw circuit was detected using a lock-in amplifier SR830 and used to calculate the sample resistance (Figures 4d-e). In this approach, all constant voltage contributions associated with thermoelectric phenomena (thermo EMF) are filtered out by the lock-in amplifier. A similar result may be obtained by direct subtraction the resistance data obtained for different directions of DC current (Supporting Figure S19).

As a result, we found that the dependence of the electrical resistance of the sample on temperature R(T) has a significant hysteresis (Figures 4b-c) in the region of 220-230 K, which completely disappears above 235 K. Below this temperature there is a difference not only between curves with different directions of DC current (\pm 1 mA), but also between the cooling and heating curves ($\Delta T > 2$ K), which indicates the presence of a "memory" effect of the sample. When a direct current flows through the sample, it creates vortices in SC grains. These frozen vortices ^{45,46} lead to the symmetry-breaking effects and significant asymmetry ($R_+/R_- = 1.23$, at 215 K this ratio is much higher) in the sample conductivity as it observed in superconducting diodes ⁵⁸. At the same time, the effect depends on the prehistory of the sample, which stores a kind of "vortex memory" of the type of cycle (cooling or warming). The discovered diode effect is not large but is noteworthy because it opens up the possibility of creating SC diodes based on superhydrides made from LaH₁₀ at recordhigh operating temperatures above 220-230 K.

Finally, we observed interference oscillations of electrical resistance in inhomogeneous sample of DAC LS-3 using a previously developed circuit (Figure 4f). Applying of a weak modulating magnetic field of $B_{max} \sim 10$ G with a frequency of $v_0 = 0.1$ Hz expectedly showed the presence of a pronounced generation of higher harmonics up to $14v_0$ already at a temperature of 226 K (Figure 4g), which is 47 K higher than the previous result achieved with (La,Ce)H₉₋₁₀ 27 . The temperature range (< 230 K) where the generation of higher harmonics is observed coincides with the region of the diode effect. Thus, these effects are interrelated. The SQUID-like effect in (La,Sc)H₁₂ is observed at a small bias current $I_{bias} = 400 \,\mu\text{A}$, which improves the situation with heating of the sample. This is significantly less than the 1-2 mA we had to use in the case of (La,Ce)H₉₋₁₀ 27 and brings us closer to the currents applied in commercial SQUIDs ($\sim 1-10 \,\mu\text{A}$). Unfortunately, the size of the randomly formed SQUID-like contours was about 1 μ m or less as indicated by the low sensitivity of the sample to applied magnetic field (Supporting Figures S23-S24).

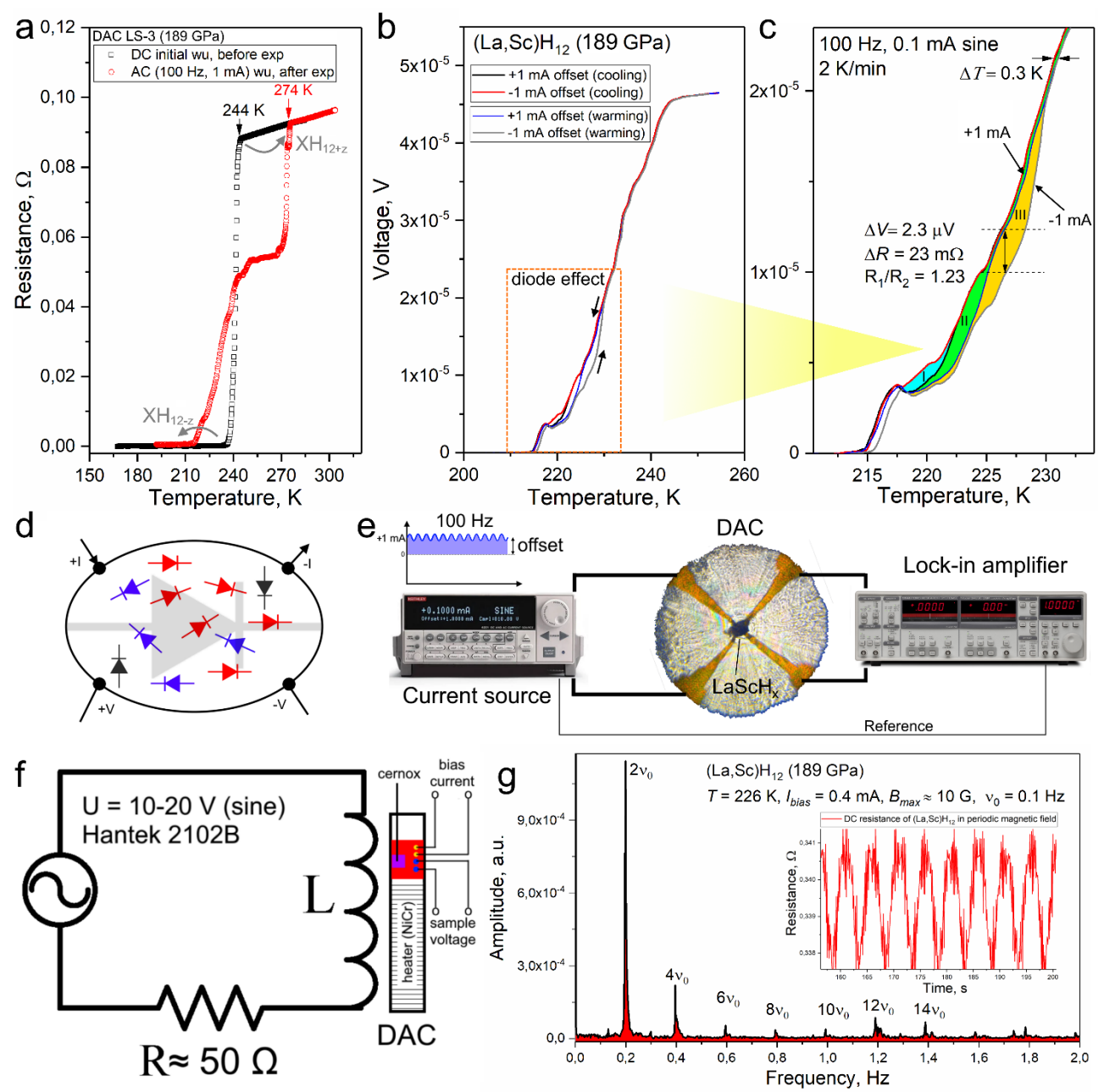


Figure 4. Diode and DC SQUID effects in (La,Sc)H₁₂ (DAC LS-3). (a) Stable (black circles) and "metastable" (red circles) resistive transitions in the La-Sc superhydride at 189 GPa. The arrows indicate a possible electrochemical process of hydrogen migration between electrodes, leading to broadening of the SC transition and the appearance of new metastable phases. (b) Diode effect observed in the sample when applying offset DC current of +/- 1 mA. Area I (azure) corresponds to the hysteresis of the sample resistance when the offset current changes its sign in a cooling cycle (2 K/min). Area II (green) corresponds to the resistance hysteresis at a constant offset +1 mA, occurring between heating and cooling cycles. Area III (yellow) corresponds to the hysteresis of the sample resistance when the current offset sign changes in the warming cycle (2 K/min). (d) Schematic illustration of the random arrangement of asymmetric conductivity regions in the sample. (e) Experimental scheme of measurements of the diode effect, which excludes the contribution of thermo EMF. (f) Scheme of studying the SQUID effect in the sample when a weak modulated magnetic field (~ 10 G) is applied. (g) Generation of higher harmonics when the (La,Sc)H₁₂ SQUID resistance changes in response to a periodic weak external magnetic field. Delta mode, which doubles the frequencies ($v_0 \rightarrow 2v_0$), was used for measurements.

Conclusions

A low-temperature (150-300 K, 153-169 GPa) X-ray diffraction study of superconducting lanthanum-scandium superhydrides ruled out phase transitions with significant symmetry changes as a possible reason for the sharp drop of electrical resistance in the sample. At 189-196 GPa we discovered new

cubic polyhydride (La,Sc) H_{12} which demonstrates the disappearance of electrical resistance on all channels of the van der Pauw four-contact circuit below 230 K. The onset critical temperature of this phase, which is dominant in our experiment, reaches $T_c = 248$ K, which is in agreement with Anderson's theorem for doped BCS-ME superconductors.

Investigation in strong steady and pulsed magnetic fields has shown that magnetoresistance of (La,Sc)H₁₂ is practically absent. Extrapolated upper critical magnetic field in some heterogeneous samples may exceed 200-230 T at 0 K. Measured Hall coefficient is negative, has no features near the T_c and in absolute value (\sim 2×10⁻¹⁰ m³/C) is close to the values known for other superhydrides.

One of the (La,Sc)H_x samples at 189 GPa demonstrated unusual "metastable" drop in electrical resistance around 274 K. This makes the La-Sc-H system very attractive for further investigation since this anomaly may have a superconducting nature. In addition, the studied (La,Sc)H_x sample demonstrates a pronounced DC SQUID-like interference oscillations of electrical resistance and diode effect at an unprecedented high temperature of about 226 K.

Acknowledgments

D. S. and D. Z. thank Beijing Natural Science Foundation (grant No. IS23017) and National Natural Science Foundation of China (NSFC, grant No. 12350410354) for support of this research. D. Z. thanks China Postdoctoral Science Foundation (Certificate No. 2023M740204) and finical support from HPSTAR. D.S. and D.Z. are grateful for financial support from the EMFL-ISABEL project. The high-pressure experiments were supported by the Russian Science Foundation (Project No. 22-12-00163). XRF analysis was performed using the equipment of the Shared Research Center of the Kurchatov Complex of Crystallography and Photonics. A portion of this work was performed on the Steady High Magnetic Field Facilities, High Magnetic Field Laboratory (CAS). All authors thank the staff scientists of the SPring-8, Elettra, Xpress station (proposals No. 20215034 and No. 20220288) and the ESRF, station ID27 (proposal MA-5924), synchrotron radiation facilities for their help with X-ray diffraction measurements, especially Dr. Anna S. Pakhomova (ESRF), Dr. Saori Kawaguchi (SPring-8), Dr. Boby Joseph (Elettra), Prof. Katsuya Shimizu and Dr. Yuki Nakamoto (Osaka University).

Contributions

I.A.T., D.V.S., D.Z., M.G., A.V.S., O.A.S. A.G.I., A.S.P., F.G.-A., C.X., T.H., S.L. and K.P. performed the experiments. D.Z., M.G. and D.S. prepared theoretical part of the paper. K.S.P. prepared the La—Sc alloys. A.G.I. analyzed composition of La-Sc alloys. I.A.T. prepared diamond anvil cells for experiments. A.V.S., O.A.S., and V.M.P. performed the magnetotransport experiments in magnetic fields below 16 T and participated in the data processing and discussions. W.C. wrote scripts for critical current measurements. C.X. helped with Hall measurements in steady magnetic fields up to 33 T. T.H. and S.L. assisted in research in pulsed magnetic fields up to 68 T. A.S.P. and F.G.-A. performed X-ray diffraction studies. D.V.S., V.M.P. and V.V.S. wrote the manuscript. All the authors discussed the results and offered useful inputs.

Data availability

Authors declare that the main data supporting our findings of this study are contained within the paper and Supporting Information. All relevant data are available from the corresponding authors upon request.

Code availability

Quantum ESPRESSO code is free for academic use and available after registration on https://www.quantum-espresso.org/. Vienna ab-initio Simulation Package (VASP) code is available after registration on https://www.vasp.at/. USPEX code is free for academic use and available after registration on https://uspex-team.org/en/.

References

- Troyan, I. A. *et al.* High-temperature superconductivity in hydrides. *Phys. Usp.* **65**, 748-761, (2022).
- Troyan, I., Semenok, D., Sadakov, A., Lyubutin, I. & Pudalov, V. Progress, problems and prospects of room-temperature superconductivity. *JETP* **139**, 1, (2024).
- Drozdov, A. P., Eremets, M. I., Troyan, I. A., Ksenofontov, V. & Shylin, S. I. Conventional superconductivity at 203 kelvin at high pressures in the sulfur hydride system. *Nature* **525**, 73-76, (2015).
- 4 Troyan, I. A. *et al.* Anomalous High-Temperature Superconductivity in YH₆. *Adv. Mater.* **33**, 2006832, (2021).
- 5 Drozdov, A. P. *et al.* Superconductivity at 250 K in lanthanum hydride under high pressures. *Nature* **569**, 528-531, (2019).
- 6 Chen, S. *et al.* Superior Superconducting Properties Realized in Quaternary La–Y–Ce Hydrides at Moderate Pressures. *J. Am. Chem. Soc.*, (2024).
- 7 Semenok, D. V., Altshuler, B. L. & Yuzbashyan, E. A. Fundamental limits on the electronphonon coupling and superconducting *T_c*. *arXiv*:2407.12922, (2024).
- 8 Trachenko, K., Monserrat, B., Hutcheon, M. & Pickard, C. J. Upper bounds on the highest phonon frequency and superconducting temperature from fundamental physical constants. *arXiv:2406.08129*, (2024).
- 9 Sadovskii, M. V. Upper Limit for Superconducting Transition Temperature in Eliashberg–McMillan Theory. *JETP Letters*, (2024).
- Anderson, P. W. Theory of dirty superconductors. J. Phys. Chem. Solids 11, 26-30, (1959).
- Gor'kov, L. P. *Theory of Superconducting Alloys*, in *Superconductivity: Conventional and Unconventional Superconductors* 201-224 (eds K. H. Bennemann & John B. Ketterson) (Springer Berlin Heidelberg, 2008).
- Semenok, D. V. *et al.* Effect of Magnetic Impurities on Superconductivity in LaH₁₀. *Adv. Mater.* **34**, 2204038, (2022).
- Semenok, D. V. *et al.* Superconductivity at 253 K in lanthanum-yttrium ternary hydrides. *Mater. Today* **48**, 18-28, (2021).
- Bi, J. *et al.* Stabilization of superconductive La-Y alloy superhydride with *Tc* above 90 K at megabar pressure. *Mater. Today Phys.*, 100840, (2022).
- 15 Chen, S. *et al.* Synthesis and superconductivity in (La, Ca) H₁₀ under high pressure. *Phys. Rev. B* **109**, 224510, (2024).
- Zhang, K. *et al.* High-pressure synthesis of a ternary yttrium-sulfur hydride superconductor with a high T_c of approximately 235 K. *Sci. China: Phys., Mech. Astron.* **67**, 238211, (2024).
- 17 Chen, S. *et al.* High-temperature superconductivity up to 223 K in the Al stabilized metastable hexagonal lanthanum superhydride. *Natl. Sci. Rev.* **nwad107**, (2023).
- Song, Y. *et al.* Stoichiometric Ternary Superhydride LaBeH₈ as a New Template for High-Temperature Superconductivity at 110 K under 80 GPa. *Phys. Rev. Lett.* **130**, 266001, (2023).
- 19 Chen, L.-C. *et al.* Synthesis and superconductivity in yttrium-cerium hydrides at high pressures. *Nat. Commun.* **15**, 1809, (2024).
- 20 Chen, W. *et al.* Enhancement of superconducting critical temperature realized in La-Ce-H system at moderate pressures. *Nat. Commun.* **14**, 2660, (2023).
- Bi, J. *et al.* Giant enhancement of superconducting critical temperature in substitutional alloy (La,Ce)H₉. *Nat. Commun.* **13**, 5952, (2022).
- Song, X. et al. Superconductivity above 105 K in Nonclathrate Ternary Lanthanum Borohydride below Megabar Pressure. J. Am. Chem. Soc., (2024).

- Guo, J. *et al.* Stabilization of high-temperature superconducting A15 phase La₄H₂₃ below 100 GPa. *Natl. Sci. Rev.* **Accepted**, (2024).
- 24 Cross, S. *et al.* High-temperature superconductivity in La₄H₂₃ below 100 GPa. *Phys. Rev. B* **109**, L020503, (2024).
- Jiang, Q. *et al.* Prediction of Room-Temperature Superconductivity in Quasi atomic H₂-Type Hydrides at High Pressure *arXiv*: 2302.02621, (2023).
- He, X. *et al.* Predicted hot superconductivity in LaSc₂H₂₄ under pressure. *Proc. Natl. Acad. Sci.* **121**, e2401840121, (2024).
- Semenok, D. V. *et al.* Observation of the Josephson effect in superhydrides: DC SQUID based on (La, Ce) H₁₀ with operating temperature of 179 K. *arXiv*:2404.09199, (2024).
- Troyan, I. A. *et al.* Non-Fermi-Liquid Behavior of Superconducting SnH₄. *Adv. Sci.* **2303622**, 1-10, (2023).
- Semenok, D. Computational design of new superconducting materials and their targeted experimental synthesis Doctoral program in matraials science and engineering thesis thesis, Skoltech, (2022).
- Shao, M. *et al.* Superconducting ScH₃ and LuH₃ at Megabar Pressures. *Inorg. Chem.* **60**, 15330-15335, (2021).
- 31 Kuzovnikov, M. A. *et al.* Crystal structures of novel lanthanum superhydrides in 57th EHPRG (2019).
- Laniel, D. *et al.* High-pressure synthesis of seven lanthanum hydrides with a significant variability of hydrogen content. *Nat. Commun.* **13**, 6987, (2022).
- Geballe, Z. M. *et al.* Synthesis and Stability of Lanthanum Superhydrides. *Angew. Chem. Int. Ed.* **57**, 688 –692, (2017).
- Hirsch, J. E. Electrical Resistance of Hydrides Under High Pressure: Evidence of Superconductivity or Confirmation Bias? *J. Supercond. Nov. Magn.* **36**, 1495-1501, (2023).
- Hou, P., Belli, F., Bianco, R. & Errea, I. Quantum anharmonic enhancement of superconductivity in P6₃/mmc ScH₆ at high pressures: A first-principles study. *J. Appl. Phys.* **130**, 175902, (2021).
- Zhou, D. *et al.* Raisins in a Hydrogen Pie: Ultrastable Cesium and Rubidium Polyhydrides. *Adv. Energy Mater.* **14**, 2400077, (2024).
- Oganov, A. R. & Glass, C. W. Crystal structure prediction using ab initio evolutionary techniques: Principles and applications. *J. Chem. Phys.* **124**, 244704, (2006).
- Lyakhov, A. O., Oganov, A. R., Stokes, H. T. & Zhu, Q. New developments in evolutionary structure prediction algorithm USPEX. *Comput. Phys. Commun.* **184**, 1172-1182, (2013).
- Oganov, A. R., Lyakhov, R. O. & Valle, M. How Evolutionary Crystal Structure Prediction Works-and Why. *Acc. Chem. Res.* **44**, 227-237, (2011).
- Wang, Y., Lv, J., Zhu, L. & Ma, Y. Crystal structure prediction via particle-swarm optimization. *Phys. Rev. B* **82**, 094116, (2010).
- Wang, Y., Lv, J., Zhu, L. & Ma, Y. CALYPSO: A method for crystal structure prediction. *Comput. Phys. Commun.* **183**, 2063-2070, (2012).
- 42 Pickard, C. J. & Needs, R. J. High-Pressure Phases of Silane. *Phys. Rev. Lett.* **97**, 045504, (2006).
- Pickard, C. J. & Needs, R. J. Ab initio Random Structure Searching. *J. Phys.: Condens. Matter* **23**, 053201, (2011).
- Hirsch, J. E. & Marsiglio, F. Nonstandard superconductivity or no superconductivity in hydrides under high pressure. *Phys. Rev. B* **103**, 134505, (2021).
- Sadakov, A. V. *et al.* Vortex Phase Dynamics in Yttrium Superhydride YH₆ at Megabar Pressures. *J. Phys. Chem. Lett.* **14**, 6666-6671, (2023).
- Sadakov, A. V. *et al.* Quasi-two-dimensional vortex matter in the ThH₁₀ superhydride. *Phys. Rev. B* **109**, 224515, (2024).
- 47 Mozaffari, S. *et al.* Superconducting phase diagram of H₃S under high magnetic fields. *Nat. Commun.* **10**, 2522, (2019).

- Minkov, V. S., Ksenofontov, V., Bud'ko, S. L., Talantsev, E. F. & Eremets, M. I. Magnetic flux trapping in hydrogen-rich high-temperature superconductors. *Nat. Phys.* **19**, 1293–1300, (2023).
- Sun, D. *et al.* High-temperature superconductivity on the verge of a structural instability in lanthanum superhydride. *Nat. Commun.* **12**, 6863, (2021).
- Talantsev, E. F. & Chistyakov, V. A-15 type superconducting hydride La₄H₂₃: Nanograined structure with low strain, strong electron-phonon interaction, and moderate level of nonadiabaticity. *Superconductor Science and Technology*, (2024).
- Talantsev, E. F. & Chistyakov, V. V. A-15 type superconducting hydride La₄H₂₃: Nanograined structure with low strain, strong electron-phonon interaction, and moderate level of nonadiabaticity. *arXiv*:2402.19384, (2024).
- 52 Semenok, D. V. *et al.* Sr-Doped Superionic Hydrogen Glass: Synthesis and Properties of SrH22. *Adv. Mater.* **34**, 2200924, (2022).
- 53 Chen, W. *et al.* Synthesis of molecular metallic barium superhydride: pseudocubic BaH₁₂. *Nat. Commun.* **12**, 273, (2021).
- 54 Semenok, D. *et al.* Evidence for Pseudogap Phase in Cerium Superhydrides: CeH₁₀ and CeH₉. *arXiv*:2307.11742v2, (2023).
- Cottam, N. D. *et al.* Quantum Nature of Charge Transport in Inkjet-Printed Graphene Revealed in High Magnetic Fields up to 60T. *Small* **20**, 2311416, (2024).
- Cucciari, A., Naddeo, D., Di Cataldo, S. & Boeri, L. NbTi: a nontrivial puzzle for the conventional theory of superconductivity. *arXiv*:2403.15196, (2024).
- Talantsev, E. F. Universal Fermi velocity in highly-compressed hydride superconductors. *Matter Radiat. Extremes* **7**, 058403, (2022).
- Moll, P. J. W. & Geshkenbein, V. B. Evolution of superconducting diodes. *Nat. Phys.* **19**, 1379-1380, (2023).

SUPPORTING INFORMATION

Ternary superhydrides under pressure of Anderson's theorem:

Near-record superconductivity in (La, Sc)H₁₂

Dmitrii V. Semenok^{1,†,*}, Ivan A. Troyan^{2,†}, Di Zhou^{1,†,*}, Andrei V. Sadakov³, Kirill S. Pervakov³, Oleg A. Sobolevskiy³, Anna G. Ivanova², Michele Galasso⁴, Frederico Gil Alabarse⁵, Wuhao Chen^{6,7}, Chuanying Xi⁸, Toni Helm⁹, Sven Luther⁹, Vladimir M. Pudalov^{3,10} and Viktor V. Struzhkin^{11,*}

¹ Center for High Pressure Science & Technology Advanced Research, Bldg. #8E, ZPark, 10 Xibeiwang East Rd, Haidian District, Beijing, 100193, China

² A.V. Shubnikov Institute of Crystallography of the Kurchatov Complex of Crystallography and Photonics, 59 Leninsky Prospekt, Moscow 119333, Russia

³ V. L. Ginzburg Center for High-Temperature Superconductivity and Quantum Materials, Moscow, 119991 Russia

⁴ Institute of Solld State Physics, University of Latvla, 8 Kengaraga str., LV-1063 Riga, Latvla

Elettra Singrature Triesto, Strada Statalo 14 km 162.5 in APEA Science Park, Pagovizza, Triesto 24140, Italy

⁵ Elettra Sincrotrone Trieste, Strada Statale 14 km163,5 in AREA Science Park, Basovizza, Trieste 34149, Italy ⁶ Department of Physics, Southern University of Science and Technology, Shenzhen 518055, China

⁷ Quantum Science Center of Guangdong-Hong Kong-Macao Greater Bay Area (Guangdong), Shenzhen, China
⁸ Anhui Province Key Laboratory of Condensed Matter Physics at Extreme Conditions, High Magnetic Field Laboratory of the Chinese Academy of Science, Hefei 230031, Anhui, China.

⁹ Hochfeld-Magnetlabor Dresden (HLD-EMFL) and Würzburg-Dresden Cluster of Excellence, Helmholtz-Zentrum Dresden-Rossendorf (HZDR), Dresden 01328, Germany

National Research University Higher School of Economics, Moscow 101000, Russia
 Shanghai Key Laboratory of Material Frontiers Research in Extreme Environments (MFree), Shanghai Advanced Research in Physical Sciences (SHARPS), Pudong, Shanghai 201203, China

*Corresponding authors: Dmitrii Semenok (<u>dmitrii.semenok@hpstar.ac.cn</u>), Di Zhou (<u>di.zhou@hpstar.ac.cn</u>) and Viktor Struzhkin (<u>viktor.struzhkin@hpstar.ac.cn</u>).

[†]These authors contributed equally.

Content

1. Methods	S2
2. Elemental analysis of La-Sc alloys	S4
3. Additional X-ray diffraction data	S5
4. Transport measurements	S8
5. Theoretical calculations	S18
6 References	\$30

1. Methods

Experiment

Crystal structure of La-Sc polyhydrides synthesized in DACs LS-1,3 were studied using the synchrotron X-ray diffraction (XRD) on the ID27 beamline with a beam of wavelength of 0.3738 Å at the European Synchrotron Research Facility (ESRF, proposal MA-5924). Low-temperature XRD in DAC LS-2 was studied on a XPRESS station of Elettra (proposal 20220288) with a beam of wavelength of 0.4957 Å in the interval of 150-300 K.

Mapping of the sample center was carried out on a 4×4 or 5×5 grids with a step of 5 microns, accumulating time was about 10 seconds per image. The experimental XRD images were integrated and analyzed using the Dioptas 0.5 software package ¹. To fit the diffraction patterns and obtain the cell parameter, we analyzed the data using Mercury 2021.2.0 ² and Jana2006 software ³, employing the Le Bail method ⁴. Analysis of the spatial distribution of hydride phases in the sample was performed using the XDI program ⁵.

The Hall measurements were carried out on a steady water-cooled WM5 magnet (HMFL, Hefei, China) with a maximum magnetic field strength of 33 Tesla. A Lakeshore 370AC resistive bridge was used to measure the resistance of La-Sc superhydride samples in AC mode. The exciting current was 1 mA (RMS, 13.7 Hz), the cooling/heating rate was 2-3 K/min, and the temperature stabilization time was 10 min for each temperature point. When studying the Hall effect (the linear dependence of resistance on the magnetic field), the temperature of the sample was reduced in steps of 5-10 K, at each temperature point the dependence R(B) was measured in the range from -33 T to +33 T, which was achieved by changing the polarity of WM5 electromagnet. To simplify the analysis of the linear dependence R(B) observed in the non-superconducting state after suppression of superconductivity by a magnetic field, we removed the data corresponding to the superconducting transition region and also subtracted the zero-field resistance R(B) from the raw data.

Resistance measurements in pulsed magnetic field were performed in a four-contact van der Pauw scheme using an alternating current of 1 mA with a frequency of 16.66 kHz and 33.33 kHz. To analyze the magnetic phase diagram, we used the real part of the impedance (Z = U/I) corrected by the phase factor so that in the superconducting state Re Z = 0. The duration of the magnetic field pulse was 150 ms, the maximum amplitude was 68 Tesla. To control the temperature, a Cernox thermometer was used, glued to the gasket with thermoconductive glue. To stabilize the sample temperature, an external heater, an insulated Ni-Cr wire of 1 m long and 50 microns in diameter, was used.

Table S1. Parameters of DACs used in high-pressure experiements.

DAC number	DAC's diameter,	Culet diameter /	Initial sample composition,	Experiments
	material of the DAC	Heated at pressure	insulating gasket	
LS-1	d = 25 mm, BeCu	50 um / 196 GPa	LaSc/AB, CaF ₂ /epoxy/W	XRD (ESRF, ID27
(electrical cell)				October 2023)
				Transport measurements
				Hall measurements (Hefei
				high magnetic field center,
				April 2024)
LS-2	d = 39 mm, BeCu	75 um / 150 GPa	LaSc/AB, CaF ₂ /epoxy/W	Low-temperature XRD
(XRD cell)				(Elettra, XPRESS,
				October 2022)
LS-3	d = 15.3 mm, NiCrAl	50 um / 189 GPa	LaSc/AB, CaF ₂ /epoxy/W	XRD (ESRF, ID 27,
(electrical cell)				October 2023)
				Pulsed magnetic fields
				(Dresden, October 2023)
LS-4	d = 25 mm, BeCu	50 um / 213-220 GPa	LaSc/AB, CaF ₂ /epoxy/W	Only transport
(electrical cell)				measurements (2024)

Theory

Computational predictions of thermodynamic stability of the (LaSc)–H phases at 150 and 30 GPa were carried out using the variable composition evolutionary algorithm USPEX $^{6-8}$. The maximum number of atoms was 44, range of search was up to (LaSc)₄H₄₀. The first generation consisting of 120 structures was produced using the random symmetric 9 and random topological 10 generators, whereas all subsequent generations (80 structures) contained 30% of random structures and 70% of those created using heredity, softmutation, and transmutation operators. The evolutionary searches were combined with structure relaxations using density functional theory (DFT) 11,12 within the Perdew–Burke–Ernzerhof functional (generalized gradient approximation) 13 and the projector augmented wave method 14,15 as implemented in the VASP code $^{16-18}$. The kinetic energy cutoff for plane waves was 600 eV. The Brillouin zone was sampled using Γ -centered k-points meshes with a resolution of $2\pi \times 0.05$ Å⁻¹. This methodology is similar the one used in our previous works 19 .

The calculations of the critical temperature of superconductivity T_c and structural relaxation of LaScH_n polyhydrides were carried out using Quantum ESPRESSO (QE) package ^{20,21}. The phonon frequencies and electron-phonon coupling (EPC) coefficients were computed using density functional perturbation theory ²², employing the plane-wave pseudopotential method and Perdew-Burke-Ernzerhof exchange-correlation La.pbe-spfn-kjpaw psl.1.0.0.UPF, functional Sc.pbe-spn-kjpaw psl.1.0.0.UPF and H.pbekjpaw psl.1.0.0.UPF pseudopotentianls were used. In our ab initio calculations of superconductivity within the optimized tetrahedron method ²³ in P4/mmm-LaScH₂₀ (200 GPa and 180 GPa) obtained by the replacement La \rightarrow Sc of 2 La atoms by 2 Sc atoms in X_4H_{40} Fm $\bar{3}m$ structure, the first Brillouin zone was sampled using a $8 \times 8 \times 8$ k-points mesh and a denser $16 \times 16 \times 16$ k-points mesh was used for electron-phonon coupling calculations. Phonons were computed on a 2× 2 × 2 shifted q-points grid. In case of Pmmm-LaScH₂₄ (193 GPa) obtained from $Pm\overline{3}m$ -Sc₂H₂₄ ²⁴ via Sc \rightarrow La substitution with corresponding relaxation, we applied 12× 12×12 k-points and $4 \times 4 \times 4$ shifted q-points grids. T_c was calculated by solving Eliashberg equations ²⁵ using the iterative self-consistent method 26 . More approximate estimates of T_c were made using the Allen–Dynes formula ²⁷.

The most important conclusion from the theoretical analysis is that the LaScH₂₀ (XH₁₀) structure has lower $T_c \sim 200\text{-}220$ K than structures with a higher hydrogen content like LaScH₂₄ (XH₁₂) which have a significantly higher T_c of about 260-280 K. Qualitatively this is consistent with experiment even though the theoretical structures have a different symmetry than the experimental phases.

2. Elemental analysis of La-Sc alloys

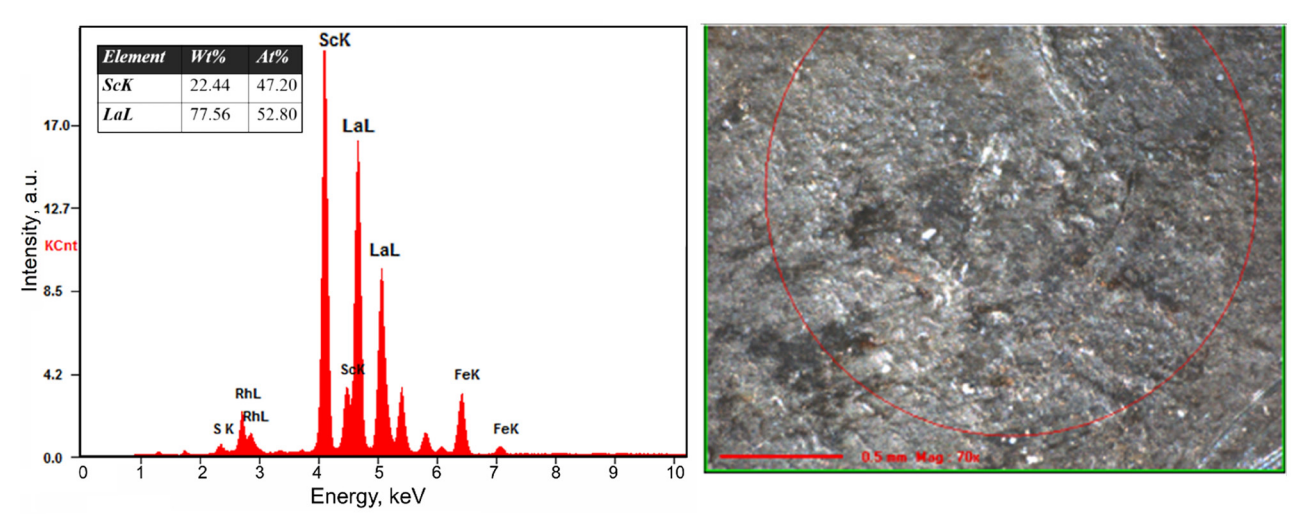


Figure S1. XRF analysis and photo of the LaSc alloy in the area marked with a red circle, where the concentration of elements was: Sc (K-line) 24.09 (weight, %) 49.50 (atom%), La (L-line) 75.91 (weight, %) 50.50 (atom %).

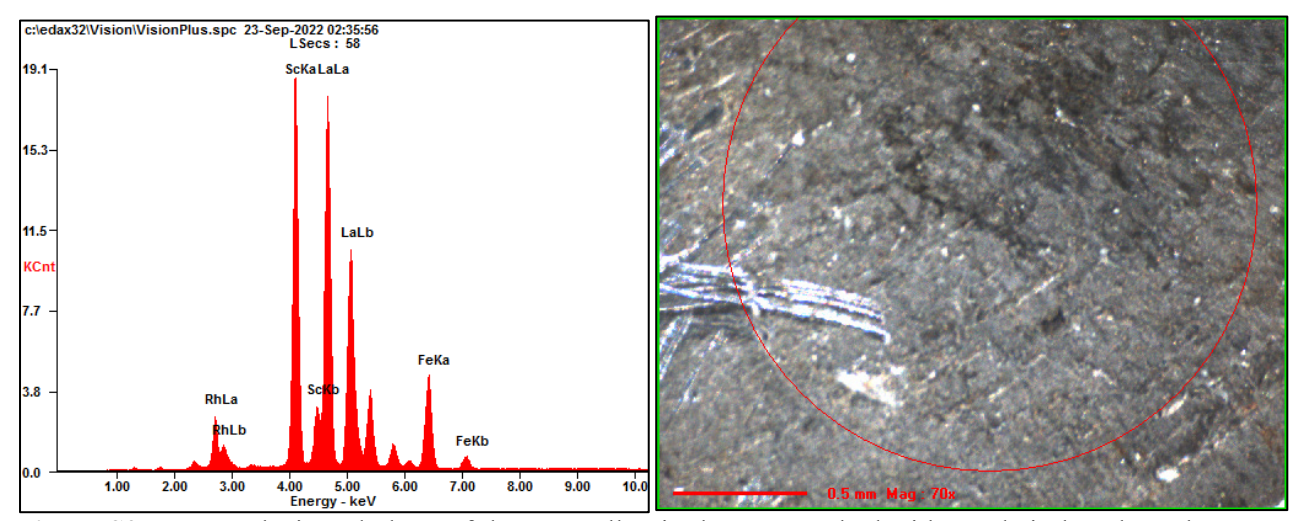


Figure S2. XRF analysis and photo of the LaSc alloy in the area marked with a red circle, where the concentration of elements was: Sc (K-line) 19.09 (weight, %) 42.17 (atom %), La (L-line) 80.91 (weight, %) 57.83 (atom %).

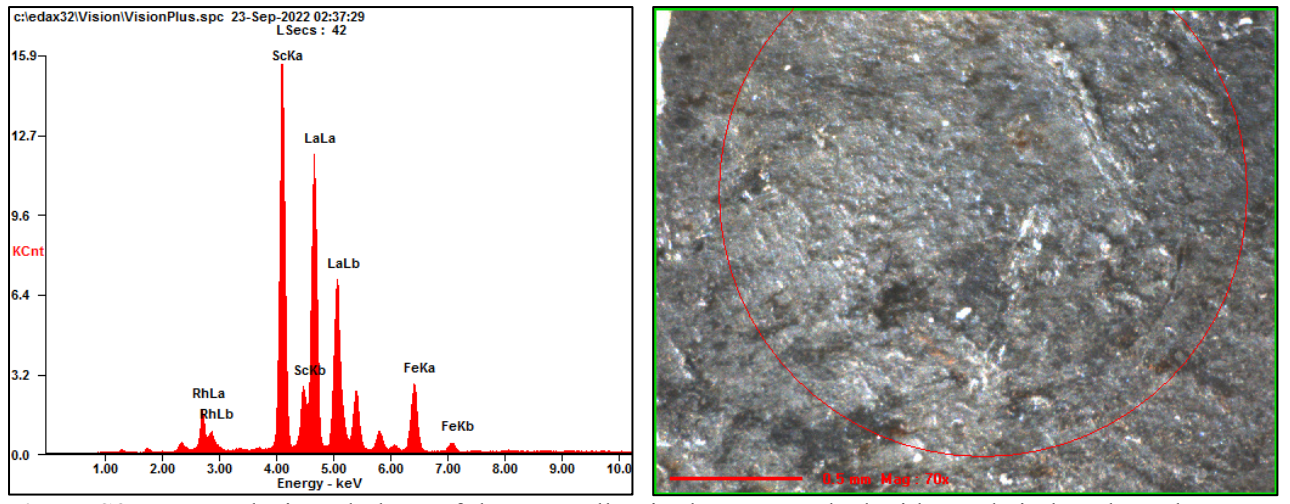


Figure S3. XRF analysis and photo of the LaSc alloy in the area marked with a red circle, where the concentration of elements was: Sc (K-line) 22.76 (weight, %) 47.65 (atom %), La (L-line) 77.24 (weight, %) 52.35 (atom %).

3. Additional X-ray diffraction data

The resulting diffraction pattern of DAC LS-1 (Figure 1) qualitatively contains "point" diffraction lines (indicated by "□" in Supporting Figure S4i), which correspond to the expected position of cubic reflections of distorted Fm3m-(La,Sc)H₁₂. Along with this ternary hydride phase, there is a redistribution of peak intensity in favor of the (002) reflection, as well as additional diffuse reflections (210) and (211) accompanying the cubic reflections (111) and (002) (Supporting Figures S4a-c, e-h), which may indicate the formation of the Fmmm-(La,Sc)H₁₂ ternary phase as well. If we include in the analysis a true ternary phase Pmmm-LaScH₂₄ with ordered La and Sc sublattices, then it shows that for any regular replacement of two La atoms by two Sc atoms in the La₄H₄₀ cell, the resulting compound will demonstrate almost the same X-ray diffraction patterns, shown in green on Supporting Figure S4j. As can be seen from this figure, there is a good agreement between the experimental diffraction pattern and the expected diffraction spectrum of the LaScH₂₄ with a regular arrangement of La and Sc atoms.

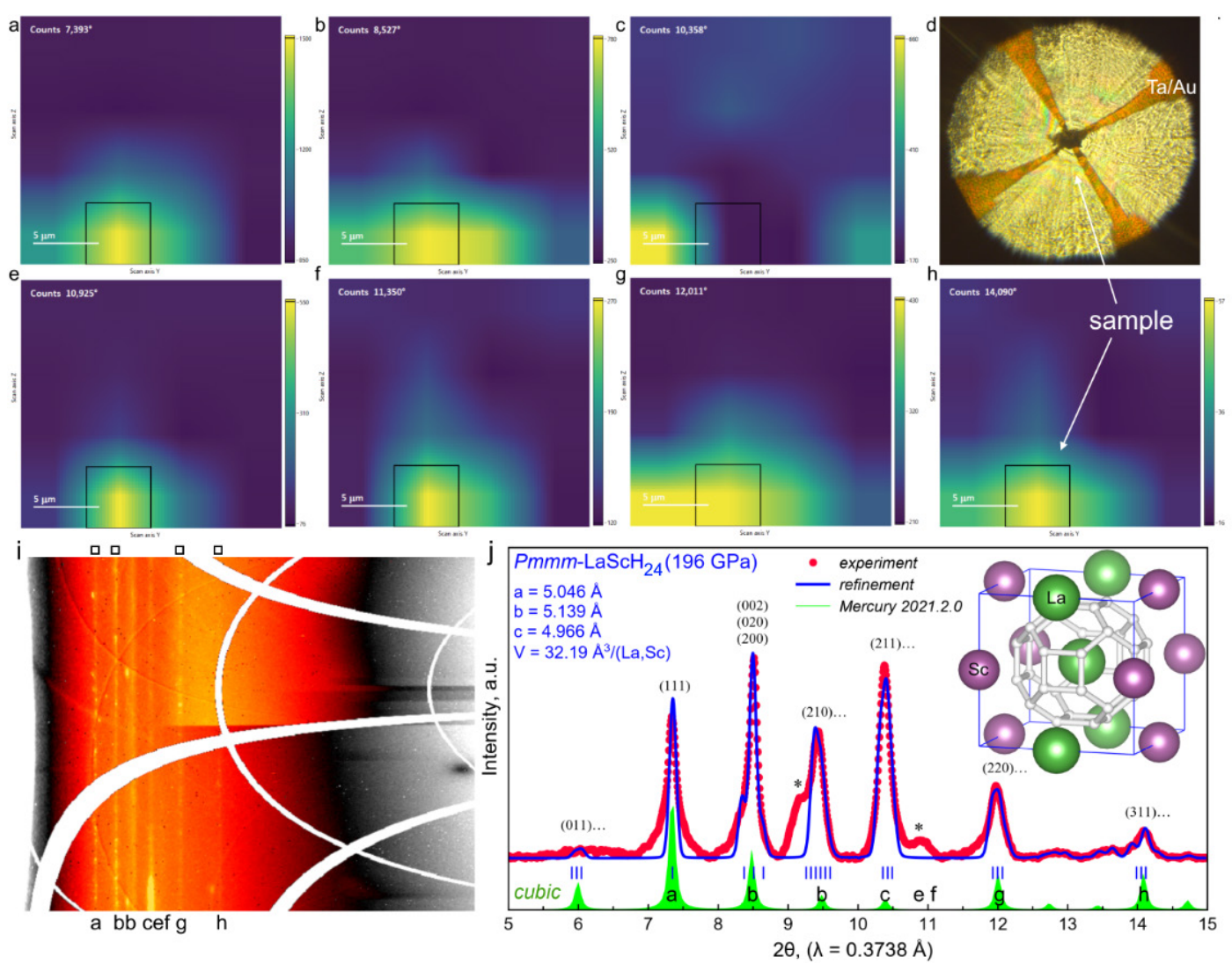


Figure S4. Powder X-ray diffraction analysis and the Le Bail refinement of the Fmmm-(La,Sc)H₁₂ (distorted cubic, pseudo $Fm\bar{3}m$) unit cell in the DAC LS-1 at 196 GPa. XRD map of the sample is shown on pictures (a-c) and (e-h) and indicates that all diffraction peaks belong to the same region of the diamond anvil (left-bottom corner). Panel (d) shows photo of the (La,Sc)H₁₂ sample on the culet with four connected Ta/Au electrodes. (i) X-ray diffraction image ("cake") of the sample. (j) Le Bail refinement of the unit cell parameters of Fmmm-(La,Sc)H₁₂ (JANA2006): red points mark experimental data, the blue line − is the refinement, the green one − is predicted XRD for undistorted cubic (La,Sc)H₁₂ obtained by regular substitution of La → Sc in the cubic $Fm\bar{3}m$ -La₂H₂₀. Asterisks mark unexplained reflections.

The fact that different reflections belong to two slightly different zones of the sample within 10 microns may indicate that the sample is multiphase and some of the *Fmmm*-(La,Sc)H₁₂ reflections actually belong to another phase, for example, to cubic (La,Sc)H₂. This is also reflected in Supporting Figure S5.

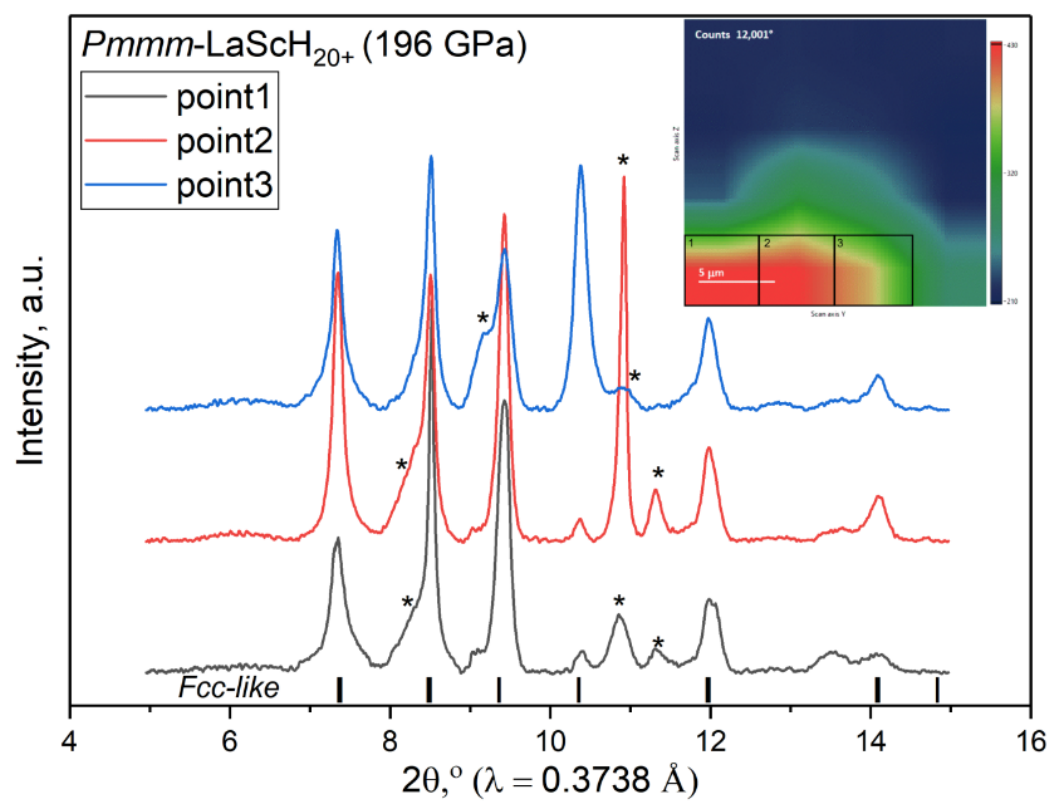


Figure S5. Powder X-ray diffraction patterns of the sample in the DAC LS-1 at 196 GPa. A series of integrated diffraction patterns at three points (#1-3) shown in the inset. Asterisks mark unexplained reflections. The positions of the expected diffraction peaks from undistorted "Fcc-like" LaScH₂₀ obtained by regular substitution of La \rightarrow Sc in the cubic $Fm\overline{3}m$ -La₄H₄₀ are shown by black dashes. From the data obtained it is clear that XRD reflections corresponding to the true ternary hydride (La,Sc)H₁₀ are present at all three points of the sample, although they have different intensities.

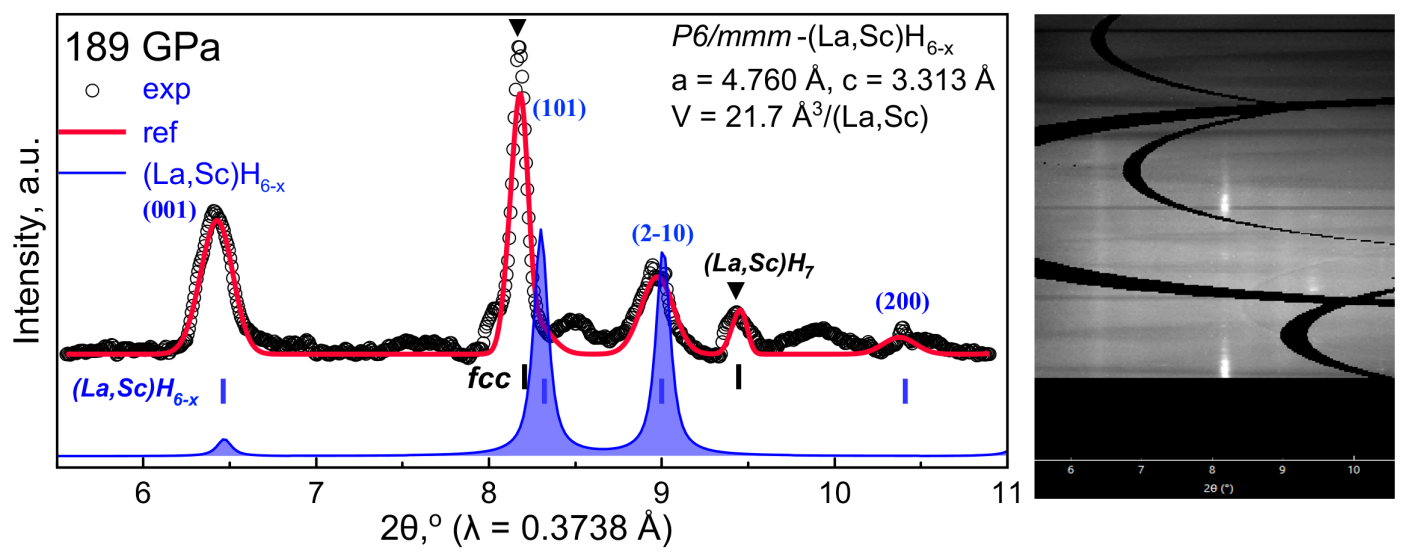


Figure S6. Powder X-ray diffraction analysis and Le Bail refinement of P6/mmm-(La,Sc)H_{6-x} and $Fm\overline{3}m$ -(La,Sc)H₋₇ in the DAC LS-3 at 189 GPa. Black points mark experimental data, the red line – is the refinement, the blue one – is predicted XRD (Mercury 2021 ²). As can be seen, the assumption of the presence of a cubic phase (La,Sc)H₋₇ with a = 4.525 Å, V = 23.16 Å³/(La,Sc) at 189 GPa makes it possible to explain some additional diffraction peaks, but significantly reduces the volume of the P6/mmm-(La,Sc)H_{6-x} phase.

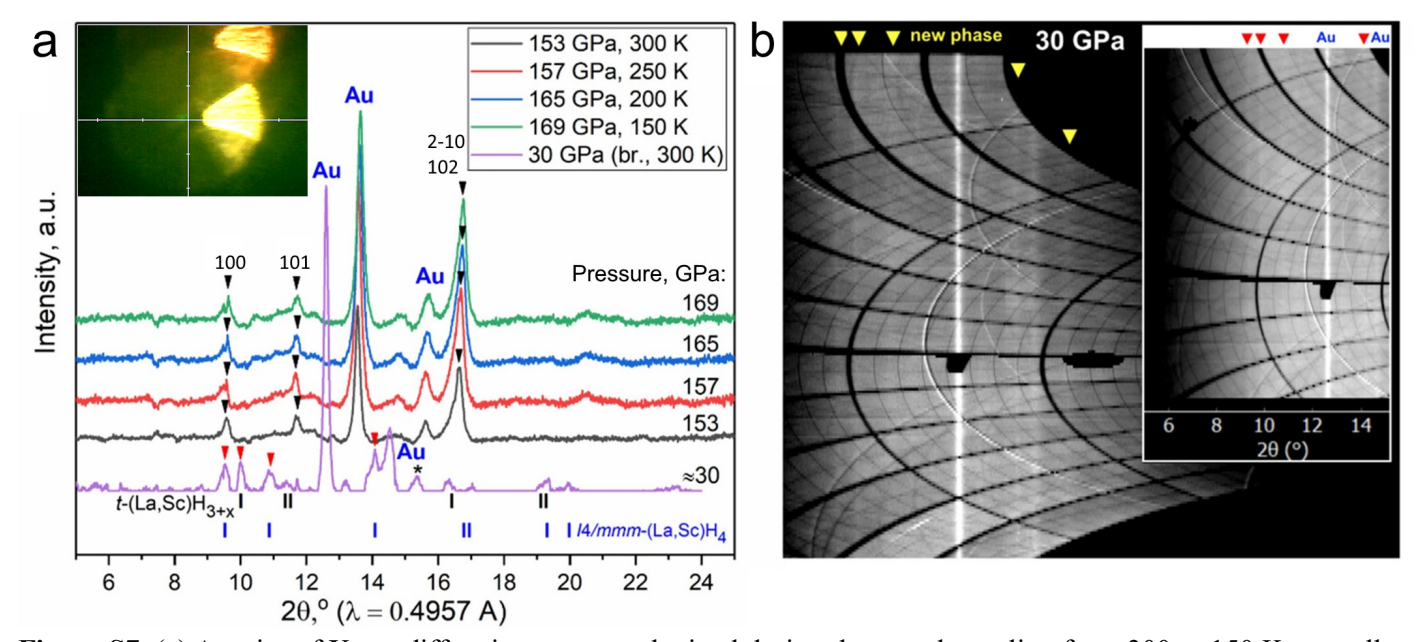


Figure S7. (a) A series of X-ray diffraction patterns obtained during the sample cooling from 300 to 150 K, as well as one XRD pattern measured after DACs failure (30 GPa). Inset: optical image of the sample in the cryostat. (b) Diffraction image obtained after the DAC collapse. The yellow triangles show reflections from the new (La,Sc)H_x phases formed when the pressure was dropped to 30 GPa.

Table S2. Unit cell parameters of I4/mmm-(La, Sc)H_{4-x} (Z = 4) and (La, Sc)H₃ (Z = 8). Due to the low intensity of the diffraction pattern, we do not expect to detect superstructural peaks corresponding to the scandium sublattice. Calculated unit cell volumes relate to 1:1 La:Sc ratio.

Pressure, GPa	Possible structural	a, Å	c, Å	V _{exp} , Å ³ /metal	V _{DFT} , Å ³ /metal
	solution			atom	atom
30	<i>I</i> 4/ <i>mmm</i> -(La, Sc)H _{4-x}	2.890	6.010	25.08	28.88
					29.01*
30	P4 ₁ -(La, Sc)H _{3-x}	4.903	9.950	29.89	33.09
	$Fm\overline{3}m$ -(La, Sc)H ₃	4.930	-	29.94	28.24**
153 (300 K)	$P6_3/mmc$ -(La,Sc)H _{6-x}	3.424	4.306	21.85	21.0 (ScH ₆)
157 (250 K)	157 (250 K) P6 ₃ /mmc-(La,Sc)H _{6-x}		4.157	21.92	20.86 (ScH ₆)
165 (200 K)	P6 ₃ /mmc-(La,Sc)H _{6-x}	3.450	4.171	21.50	20.6 (ScH ₆)
169 (150 K)	P6 ₃ /mmc-(La,Sc)H _{6-x}	3.446	4.161	21.39	20.43 (ScH ₆)

^{*}Averaged value: $0.5 \times V(ScH_4) + 0.5 \times V(LaH_4)$

Note that in the diffraction patterns (Figure 2e), the 100 reflection looks split below 250 K, which could indicate some low-symmetry distortion. Considering the changes in lattice parameters in Table S2 for $P6_3/mmc$ -(La,Sc)H_{6-x}, first the unit cell volume increases noticeably even though the temperature is reduced from 300 K to 250 K and the pressure is increased. When the temperature is further reduced to 150 K, the parameter remains almost unchanged, but there is a visible reduction in volume due to the compression along the c-axis. This behavior may indirectly indicate a continues phase transition accompanied by some structural distortion.

^{**}Averaged value: $0.5 \times V(ScH_3) + 0.5 \times V(LaH_3)$

4. Transport measurements

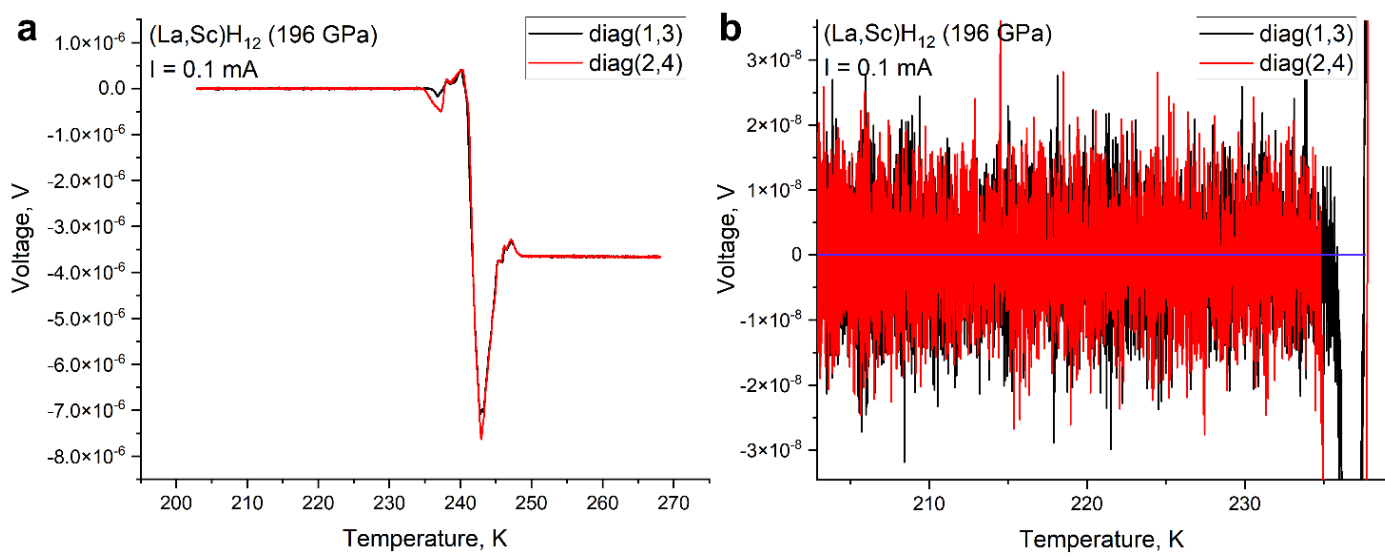


Figure S8. (a) The voltage drop across the (La,Sc) H_{12} sample at 196 GPa (DAC LS-1) measured in the diagonal connection of the van der Pauw circuit diag(1,3) and diag(2,4). (b) Residual resistance of the sample after transition to the superconducting state. The current was 0.1 mA.

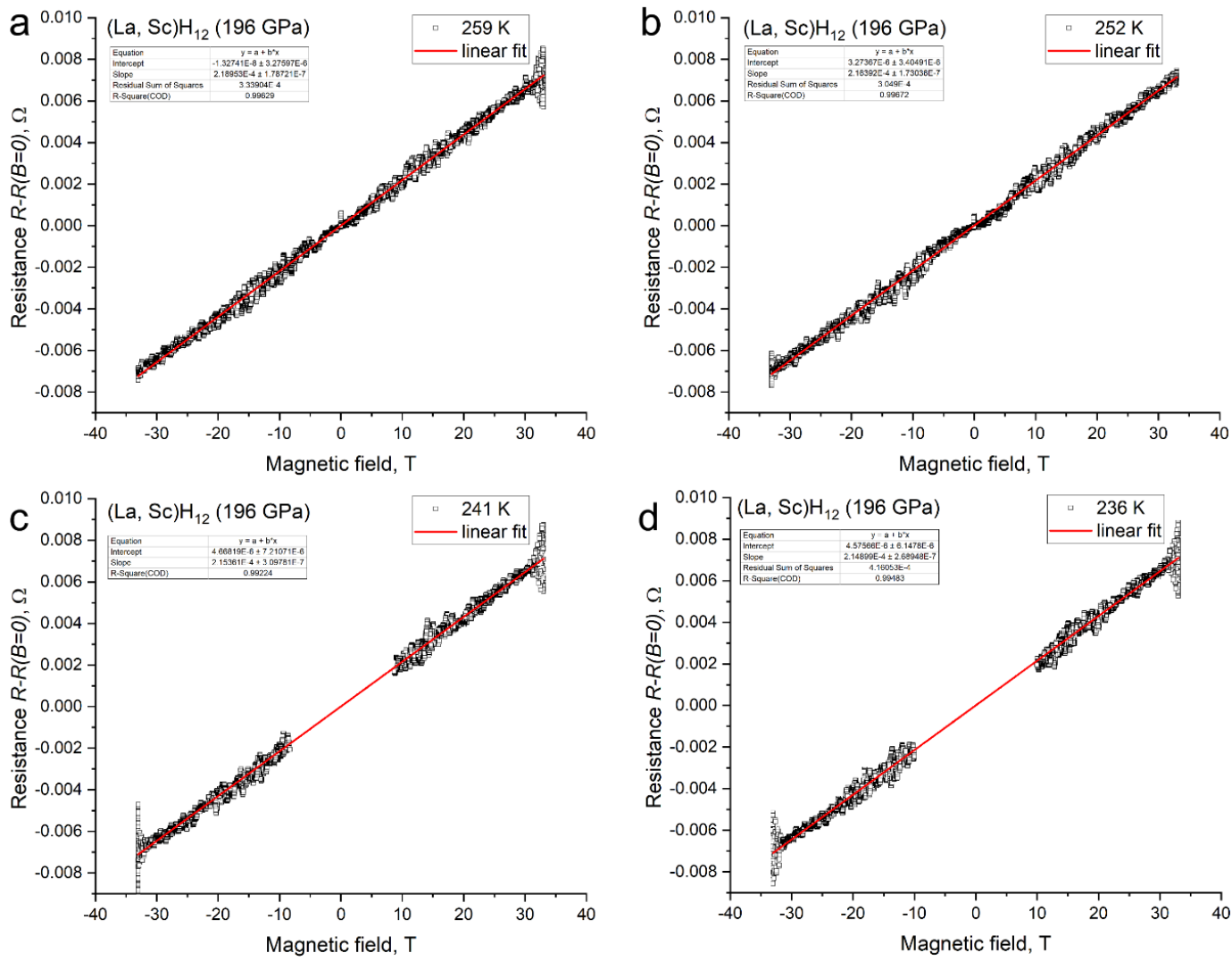


Figure S9. Hall effect in (La, Sc) H_{12} at 196 GPa (DAC LS-1) at temperatures: (a) 259 K, (b) 252 K, (c) 241 K, (d) 236 K in steady magnetic fields. The measured Hall coefficient has a negative absolute sign. Red line – is a linear fit. The central part of the R(B) curve corresponds to the region of the superconducting transition. It has been removed for clarity.

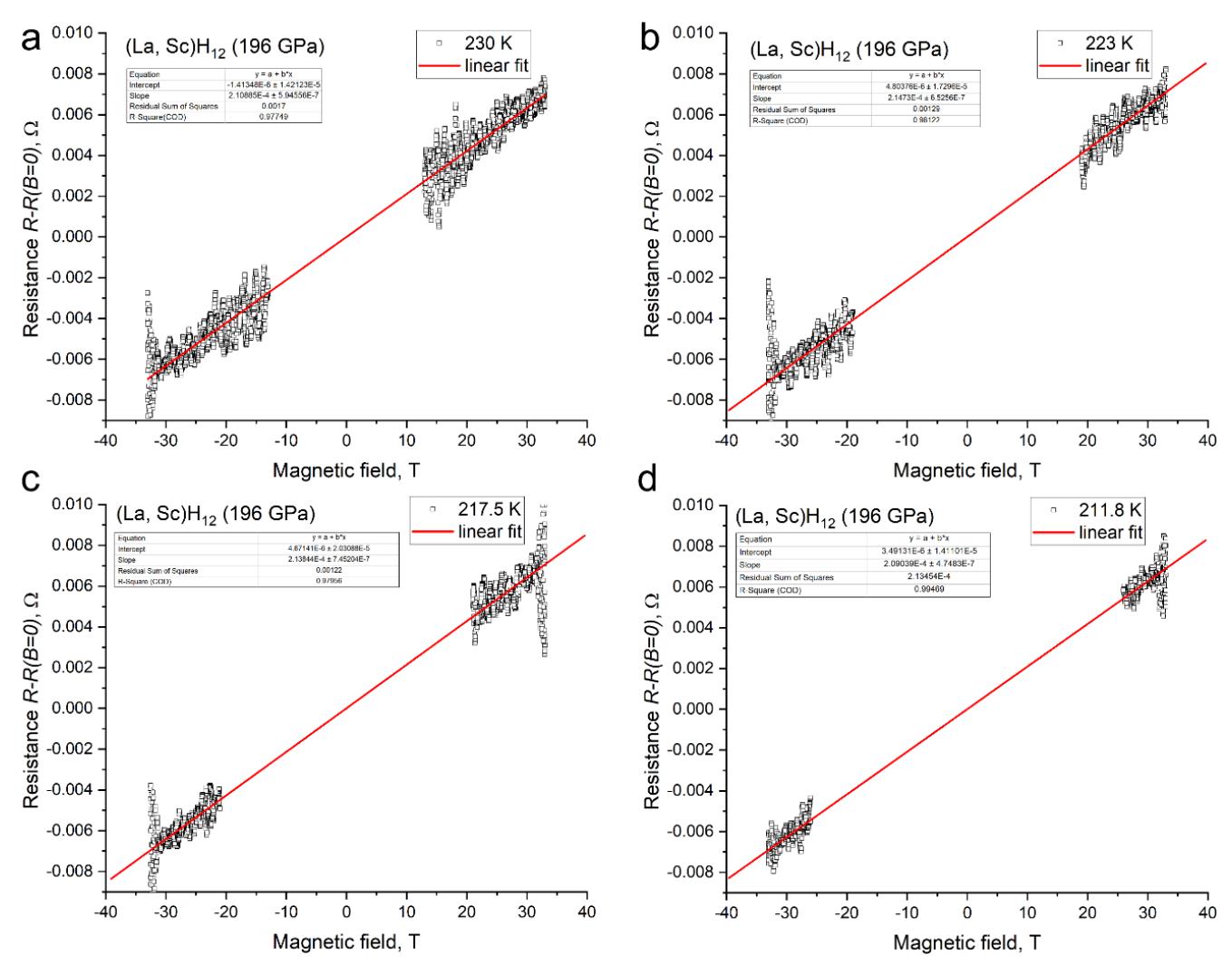


Figure S10. Hall effect in (La, Sc) H_{12} at 196 GPa (DAC LS-1) at temperatures: (a) 230 K, (b) 223 K, (c) 217.5 K and (d) 211.8 K in steady magnetic fields. The measured Hall coefficient has a negative absolute sign. Red line – is a linear fit. The central part of the R(B) curve corresponds to the region of the superconducting transition. It has been removed for clarity.

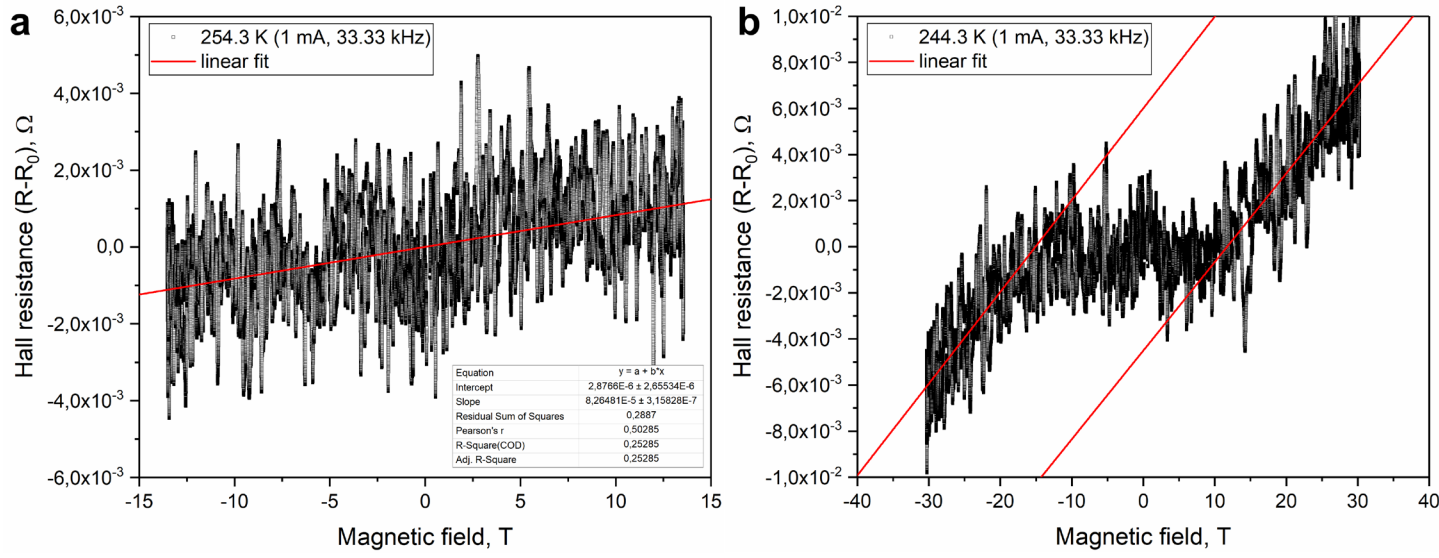


Figure S11. Hall effect measurements in (La,Sc)H₁₂ at 189 GPa (DAC LS-3) in AC mode in pulsed magnetic field at two temperature points: (a) 254.3 K and (b) 244.3 K. In general, pulsed measurements of the Hall coefficient are much noisier and less reliable than measurements in a steady magnetic field. The nonlinear behavior of the Hall coefficient at 244 K may be due to the appearance of an anomaly in the electrical resistance of the LS-3 sample (Supporting Figure S21).

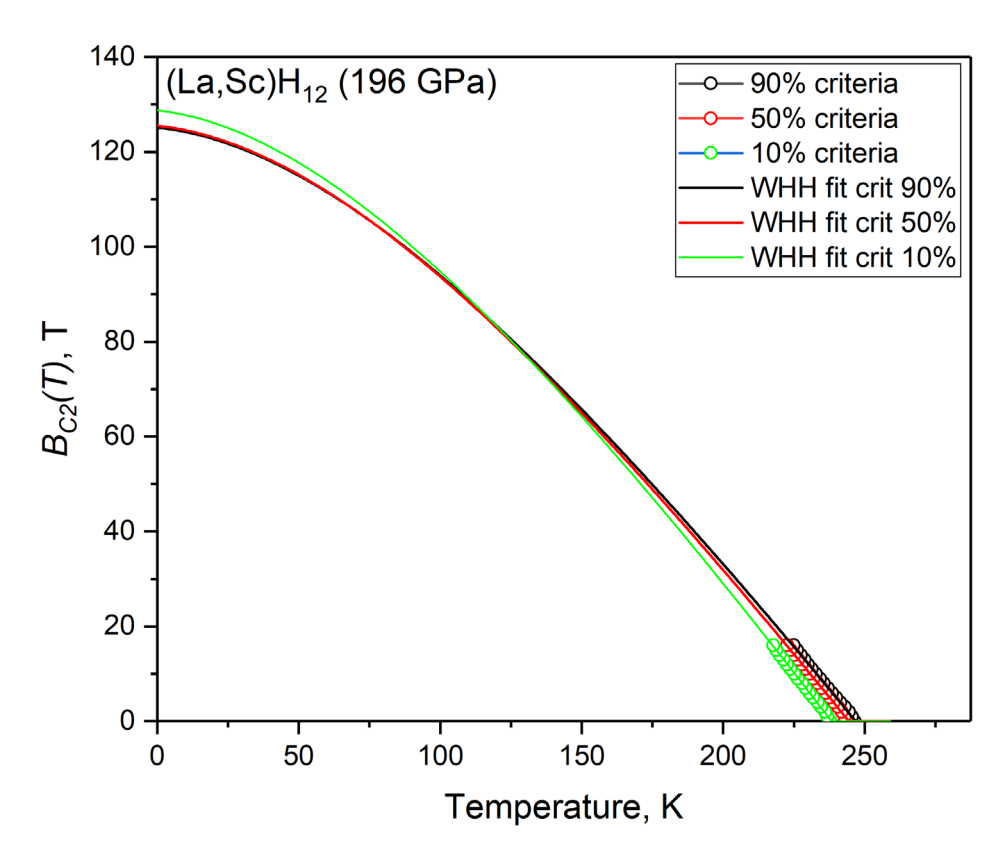


Figure S12. Extrapolation of experimental $B_{c2}(T)$ dependences to the region of strong magnetic fields for the (La,Sc)H₁₂ sample in DAC LS-1 using the simplified WHH model ²⁸. All used criteria of 90, 50, 10% of residual resistance give approximately the same $B_{c2}(0) = 125$ -130 T. The study was performed in fields up to 16 T immediately after sample synthesis (DAC LS-1, 196 GPa). This shows that the quality of the LS-1 sample is higher than that of LS-3, where the extrapolated upper magnetic field can reach 200 T and higher.

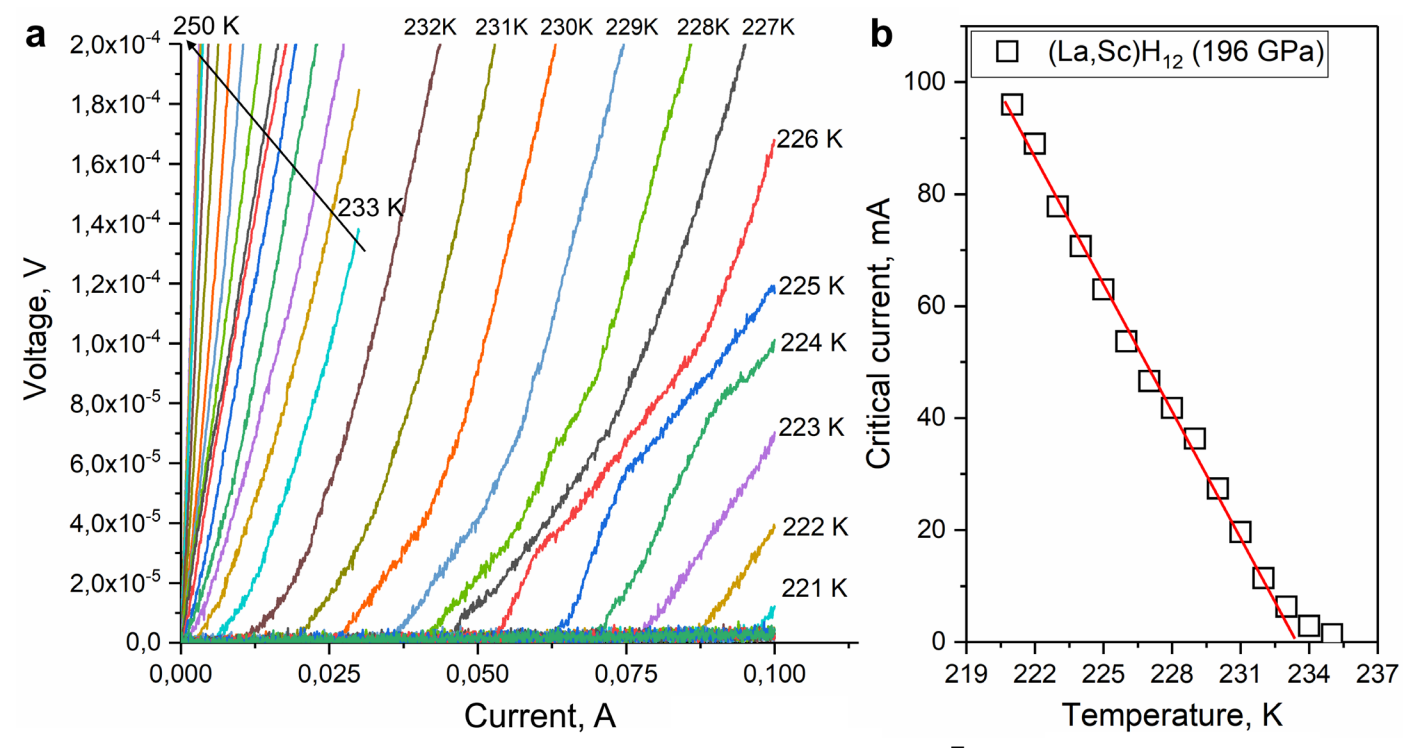


Figure S13. Current-voltage (V-I) characteristics and critical current of the $Fm\overline{3}m$ -(La,Sc)H₁₂ sample in DAC LS-1 at 196 GPa. (a) Current-voltage characteristics in the temperature range from 221 K to 250 K. V-I were taken before the degradation of the sample, which led to a broadening of the superconducting transition and a decrease in the critical current. (b) Dependence of the critical current in the (La,Sc)H₁₂ on temperature. The dependence is quasi-linear.

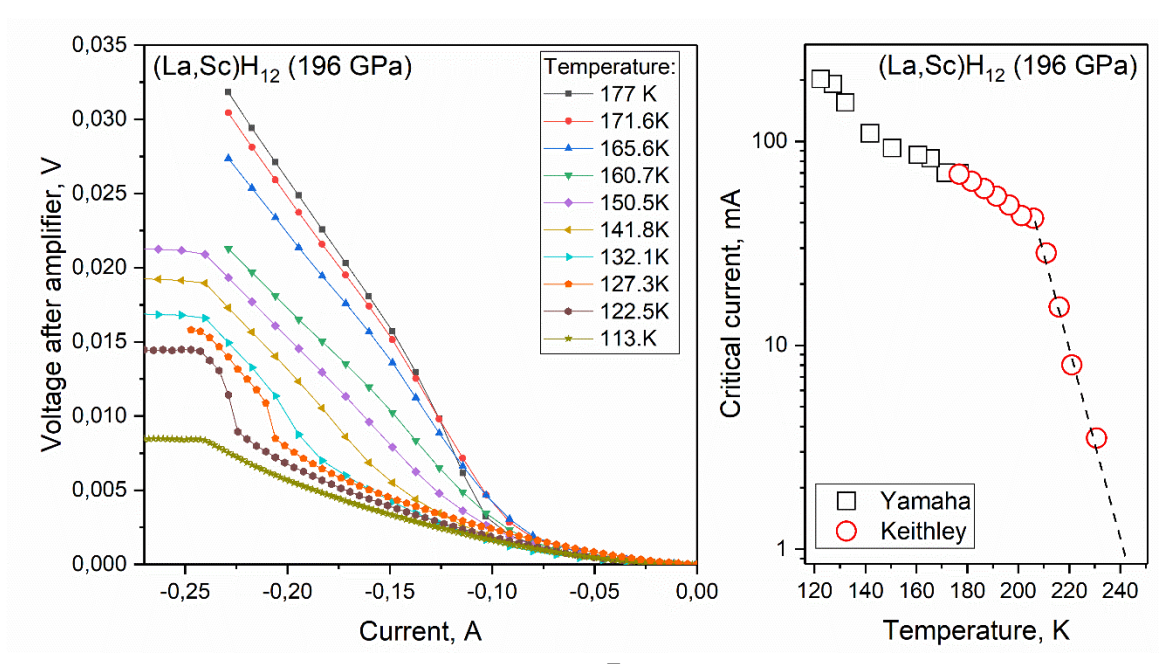


Figure S14. Current-voltage characteristics of the sample $Fm\overline{3}m$ -(La, Sc)H₁₂ (DAC LS-1) studied using a Yamaha PX-3 amplifier of pulsed Π-shaped signals generated by a Keithley 6221 source at a temperature of 113 – 177 K. The experiment was carried out after X-ray diffraction studies (degraded sample). The duration of the current pulse was 2 ms, the interval between pulses was 4-5 seconds, the result was averaged over 6 voltage values for each pulse current value. As the current increases, the sample degrades, which leads to the disappearance of the region of sharp linear increase in resistance below 122 K.

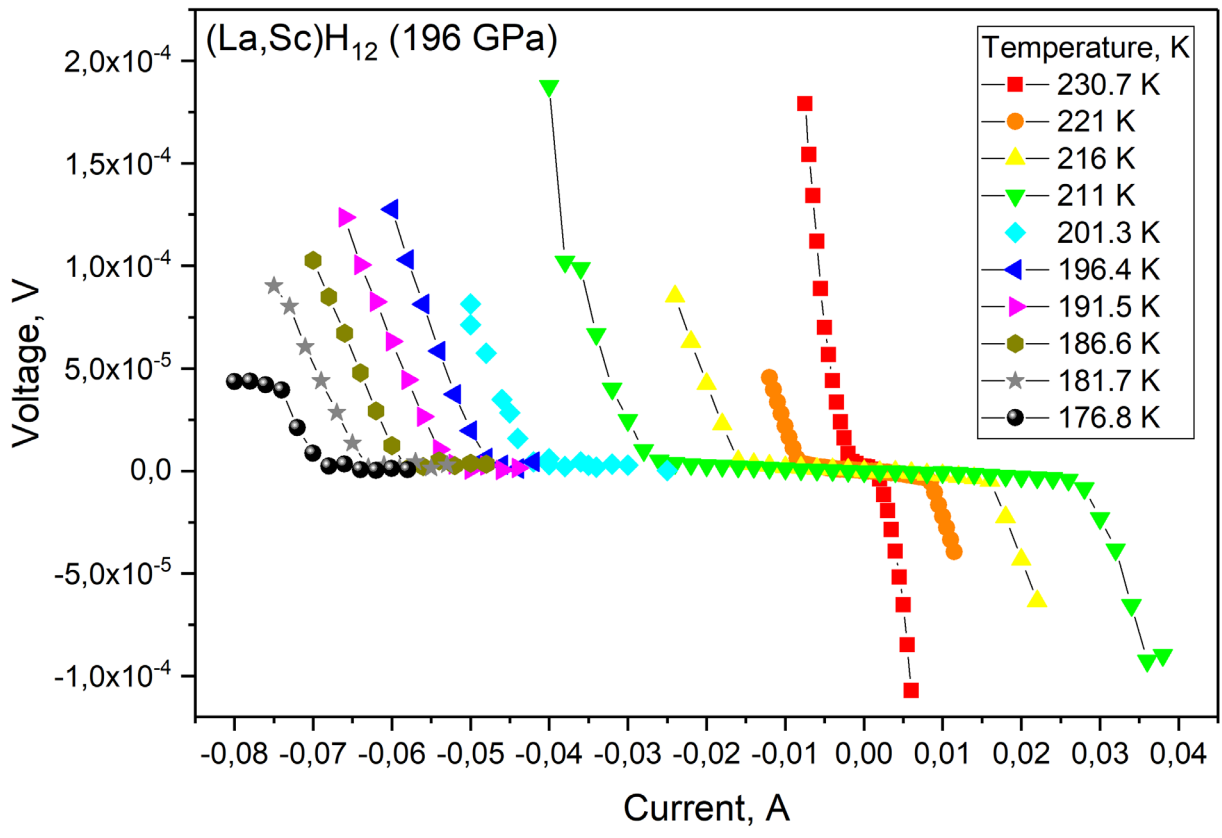


Figure S15. Current-voltage characteristics of $Fm\overline{3}m$ -(La, Sc)H₁₂ (DAC LS-1) taken in a pulsed mode using a Keithley 6221 current source. The pulse length was chosen 5 ms, averaging was carried out over 10 points, the interval between which was 1 second, and the interval between changes in the maximum pulse current value was 3 seconds. The sign of the voltage or current depends on the connection of the contacts to the sample and has no physical meaning.

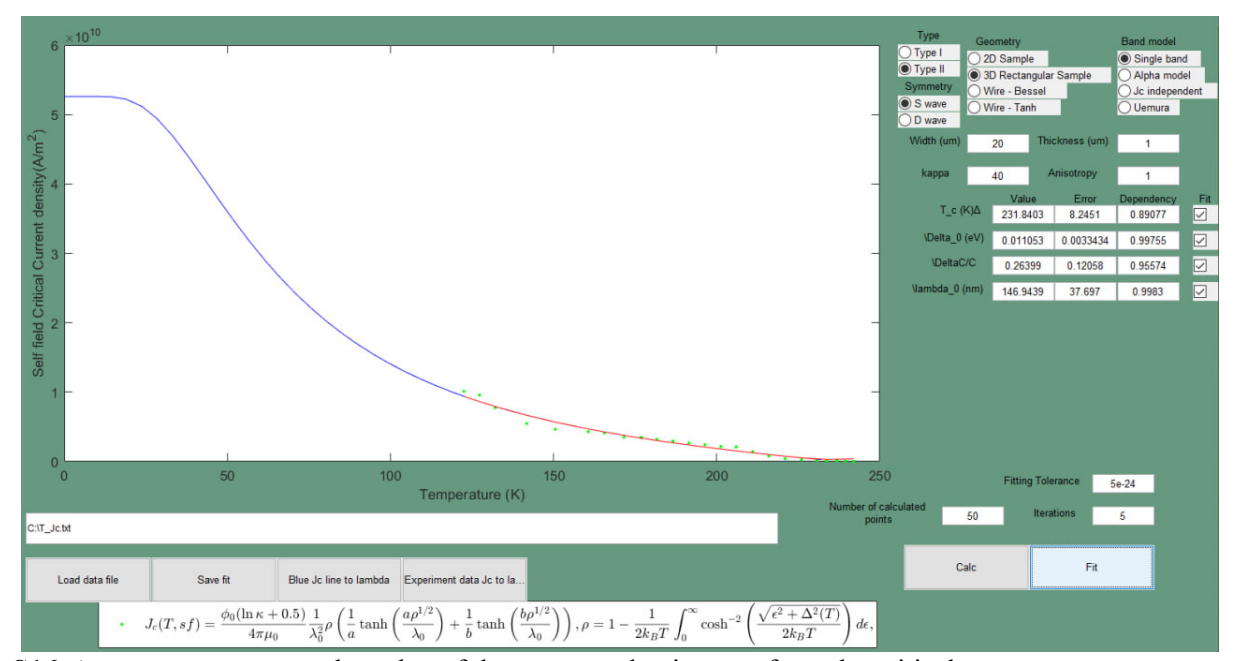


Figure S16. An attempt to extract the value of the superconducting gap from the critical current measurements using the Talantsev-Tallon method 29,30 . The obtained value of the superconducting gap is significantly lower than expected: $\Delta(0) = 11 \pm 3$ meV.

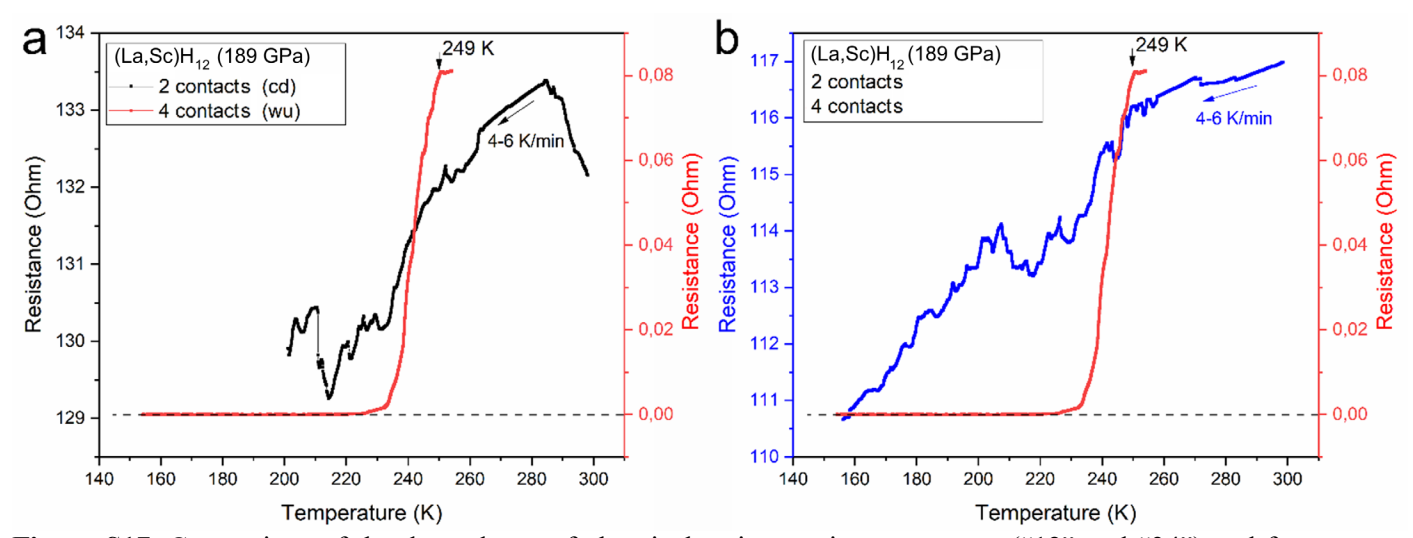


Figure S17. Comparison of the dependence of electrical resistance in two-contact ("12" and "34") and four-contact modes (van der Pauw scheme, vdP). The delta mode measurements were used, the excitation current was I=1 mA. "cd" means cooling down, "wu" means warming up. The cooling rate was chosen to be 4-6 K/min. Due to different heating and cooling rates, the superconducting transitions may be offset by \pm 5 K. Measurements in "a" and "b" panels are for different runs. It is easy to see that in two-contact scheme the superconducting transition is almost impossible to detect: R(T) behaves unpredictably.

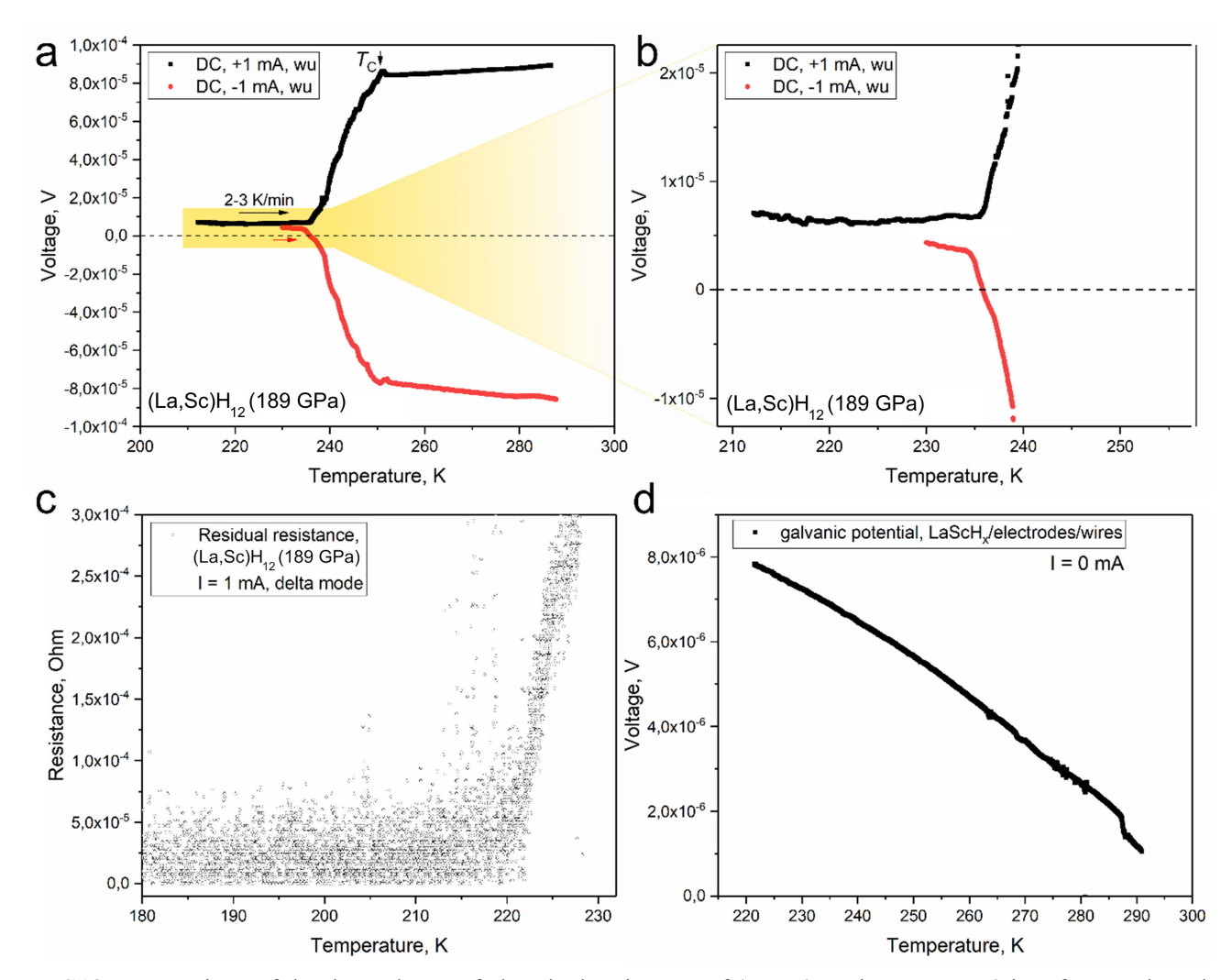


Figure S18. Comparison of the dependence of electrical resistance of (La,Sc)H₁₂ in DAC LS-3 in a four-probe scheme (van der Pauw, vdP) in DC mode (a, b) without changing the current direction, and in the delta (c) mode. (a) Dependence of the voltage drop across the sample when applying a constant current of different directions (+1 mA and -1 mA). "wu" corresponds to warming up cycle at a rate of 2-3 K/min. (c) Residual resistance of the sample measured in delta mode (I = 1 mA). At 230K the resistance is almost the same as $0.5 \times [V(+I)-V(-I)]/|I|$ from graphs (a, b). Figure (d) shows the voltage drop at zero external current, caused by the difference in contact potentials.

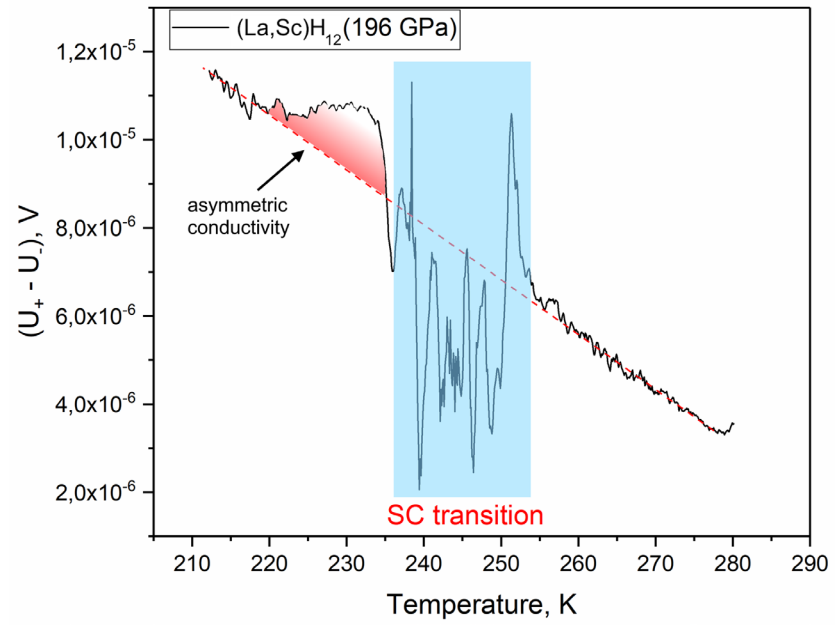


Figure S19. This figure shows that subtracting voltage measurements made using DC current ($I = \pm 1$ mA, U_+ means voltage which is measured when +1 mA current passes through) indicates the presence of deviations (conductivity asymmetry) from the linear dependence in the vicinity of the superconducting transition associated with the diode properties of the sample.

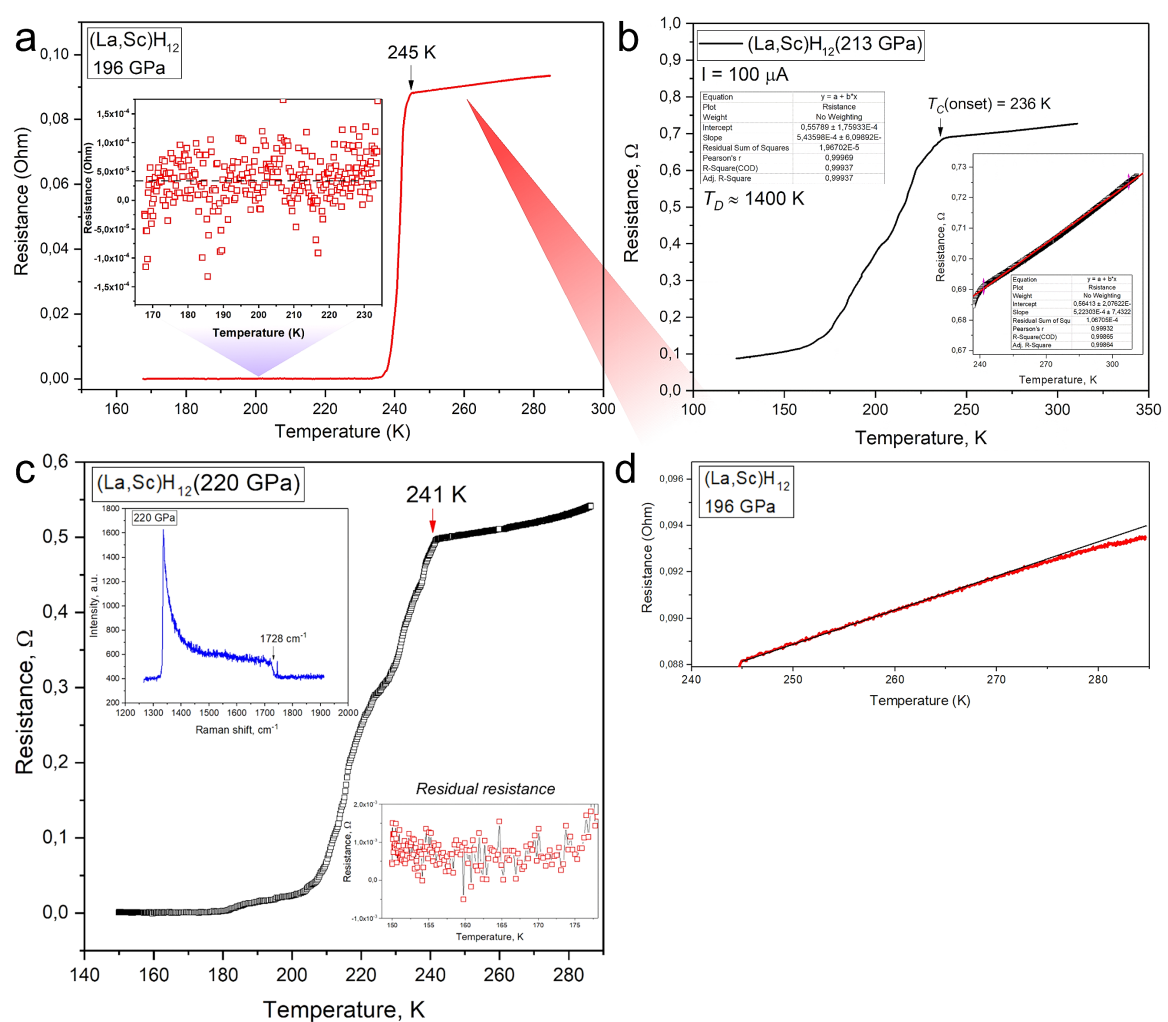


Figure S20. Superconducting transitions and temperature dependence of the electrical resistance of (La,Sc)H₁₂ at different pressures: (a) 196 GPa (DAC LS-1), (b) 213 GPa, (c) 220 GPa. In panel (b) we can see a superconducting transition in a (La,Sc)H_x sample synthesized at 213 GPa (DAC LS-4). The sample has not completely reacted with hydrogen. As a result, T_c is lower than previously found value (245 K) and there is a residual resistance below 150 K. Also, a large transition width indicates the heterogeneity of the sample. In panel (c) there is a dependence of electrical resistance on temperature for the (La,Sc)H_x sample after laser heating at 220 GPa (DAC LS-4). The Debye temperature cannot be determined reliably from this dependence since Bloch–Grüneisen (BG) fit gives $T_D > 10000$ K. Finally, in panel (d) a quasi-linear dependence of R(T) and its deviation from the BG behavior in the normal state is shown.

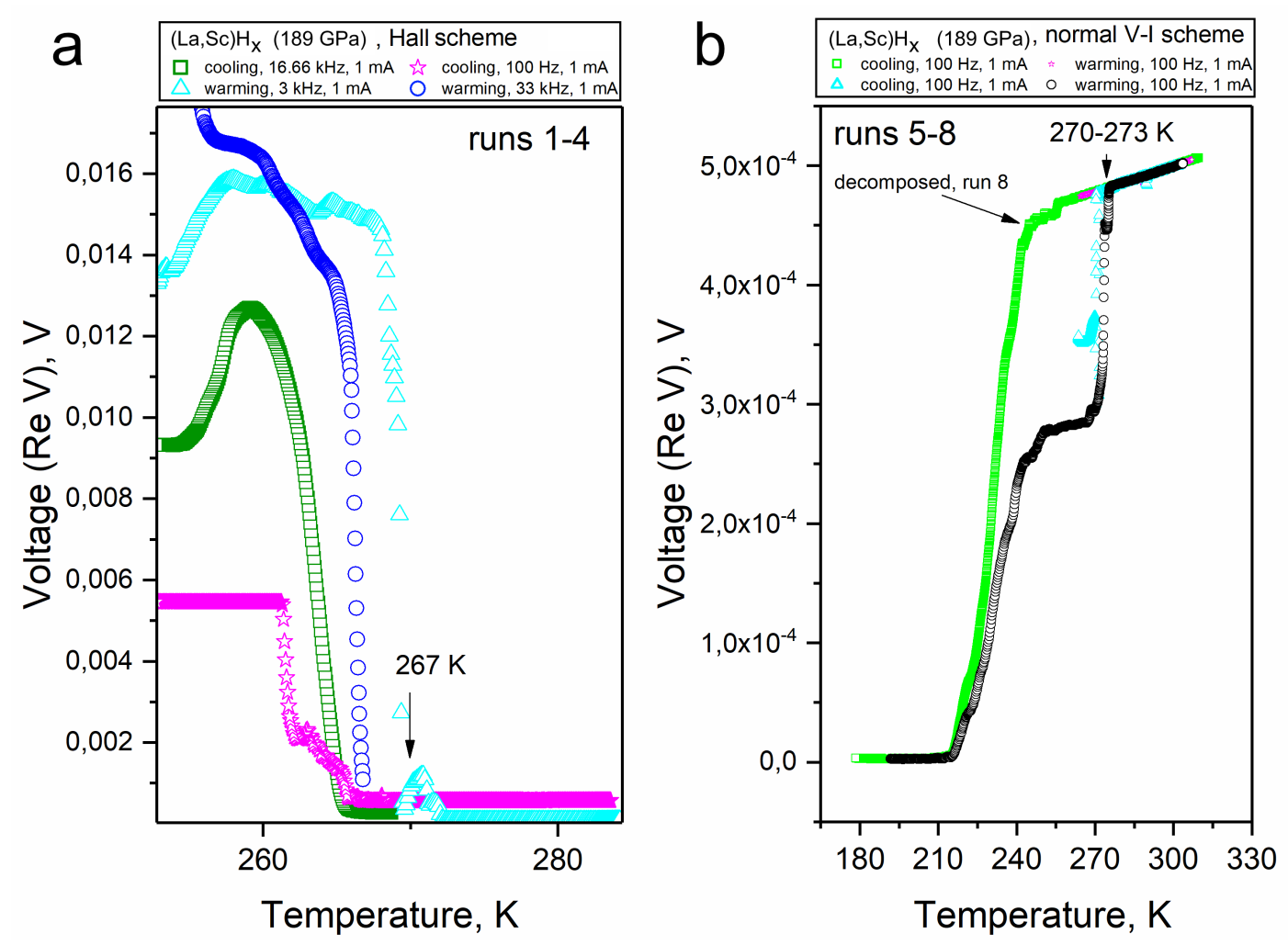


Figure S21. High temperature anomaly in the electrical resistivity of the sample at 189 GPa (DAC LS-3). (a) It was originally recorded during the study of the Hall effect, so the first 4 heating and cooling cycles (runs 1-4) were carried out in this configuration at different current frequencies (33 kHz, 16.66 kHz, 3 kHz and 100 Hz). The variation in the starting point of the anomaly may be due to the high rate of cooling and heating and the accompanying thermal hysteresis. (b) Warming up the sample in the usual V-I circuit. Current frequency 100 Hz. After a series of cooling and warming cycles, the additional drop in R(T) disappeared with the restoration of the previous resistance.

There are several possible explanations for the observed resistance anomalies:

(1) Breaks or short circuit of electrodes. In this case, we would observe a significant change in resistance, its drop to zero or large increase. Such false transitions have a limited point density.

In our case, we are dealing with only a partial change ~ 40 % in the resistance of the sample, as is the case with two-phase samples (e.g., CeH₉₋₁₀ case ³¹). Moreover, a high density of R(T) points can be achieved; the beginning and end of the anomalous resistance jump are gentle (Figure S21), which corresponds to current views on the dynamics of the vortex lattice in superhydrides ^{32,33}.

(2) A chemical, electrochemical 34 reaction or phase transition in the vicinity of one of the electrodes: $(La,Sc)H_{12} \pm nH_2 \rightarrow phase X$, with its subsequent decomposition to the initial $(La,Sc)H_{12}$.

One of the arguments in favor of this version is the detection of traces of other hexagonal phases in DAC samples LS-2, LS-3 (Figures 1e, 2c). Some of such phases were predicted to be room-temperature superconductors ³⁵.

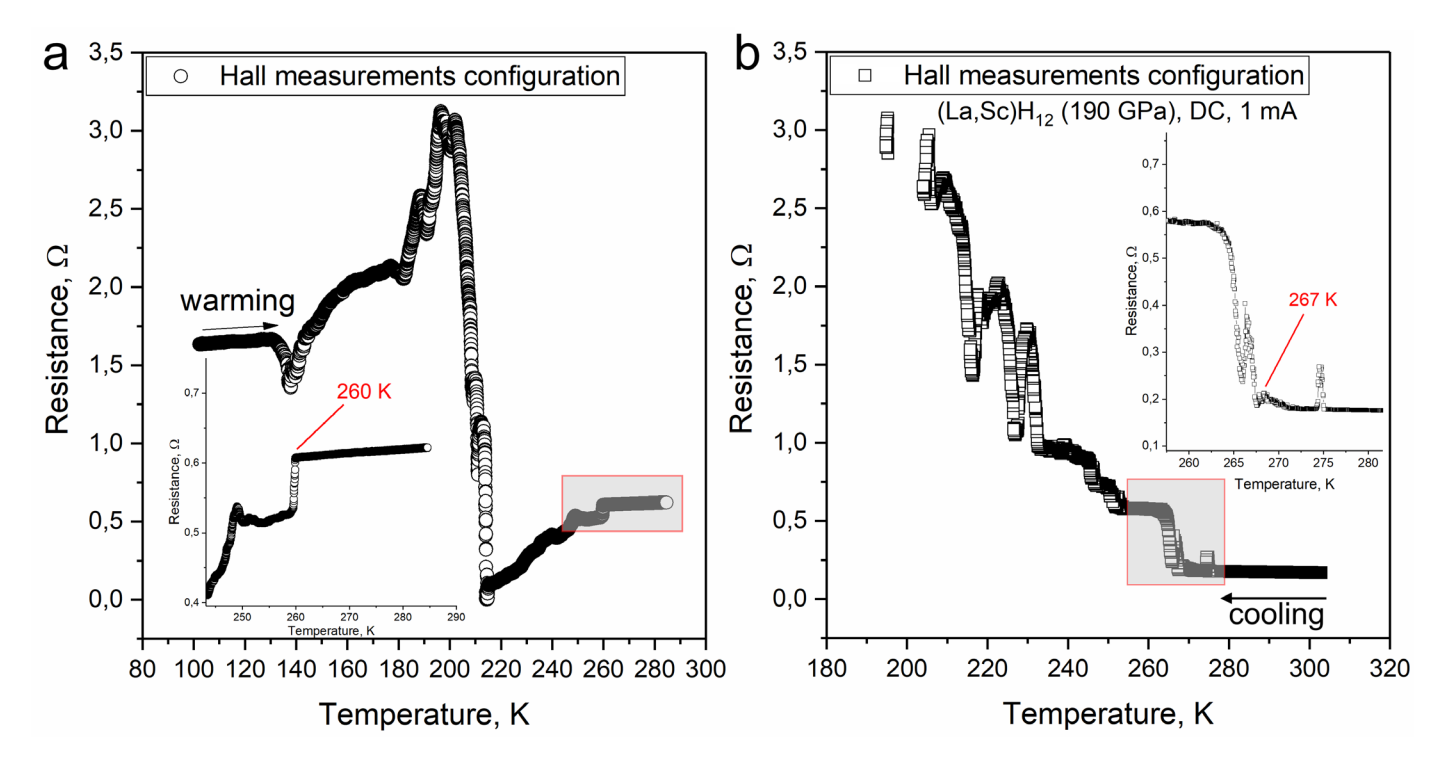


Figure S22. Hall resistance measurements in two (a, b) different diagonal connections approximately a month after the anomaly was first detected (Figure S21). As before, the beginning of the anomaly can be traced in the region of 260-267 K. After these measurements, the chamber collapsed. Because of this, it was not possible to study the behavior of this resistance anomaly in magnetic fields.

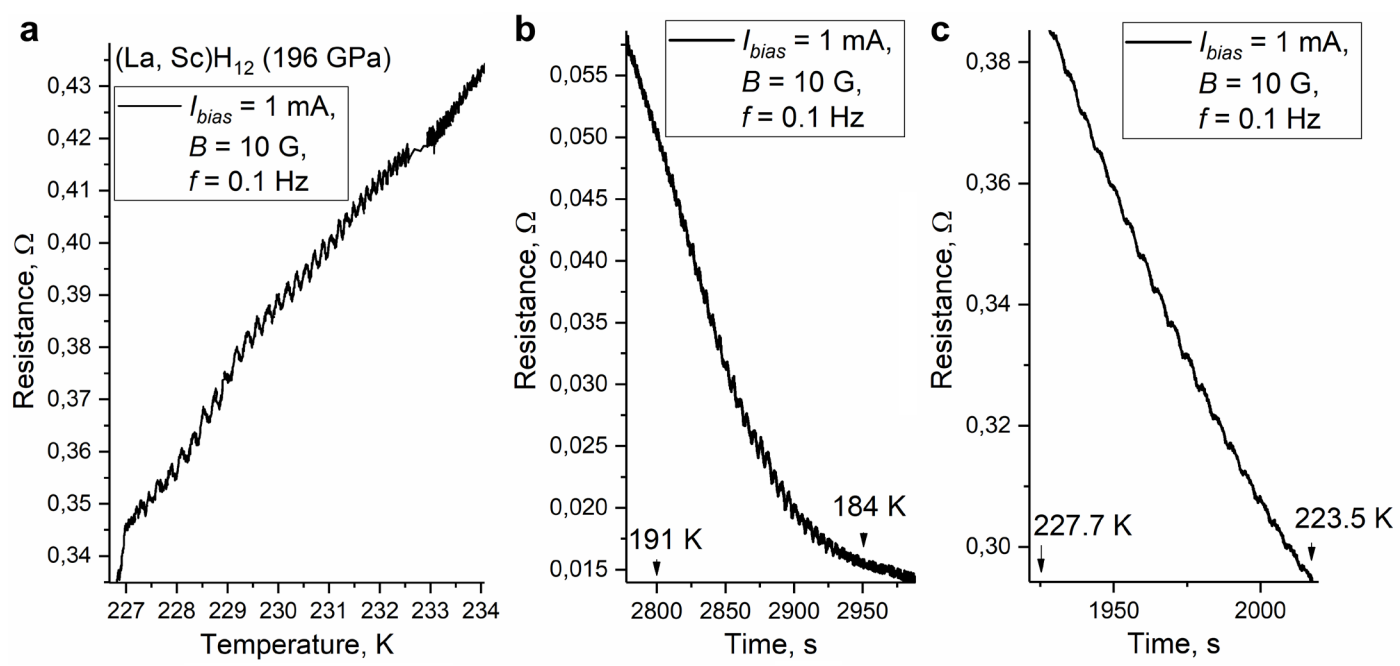


Figure S23. A SQUID-like effect in the DAC LS-3 sample upon cooling in a periodic magnetic field ~ 10 G with a frequency of 0.1 Hz. The bias current is 1 mA. The delta mode of resistance measurements was used. (a) The appearance of oscillations of electrical resistance on the R(T) dependence in the range of 227 - 232 K. (b) Similar oscillations on the dependence of resistance on time between 191 K and 184 K. (c) Weak oscillations of electrical resistance between 227.7 K and 223.5 K.

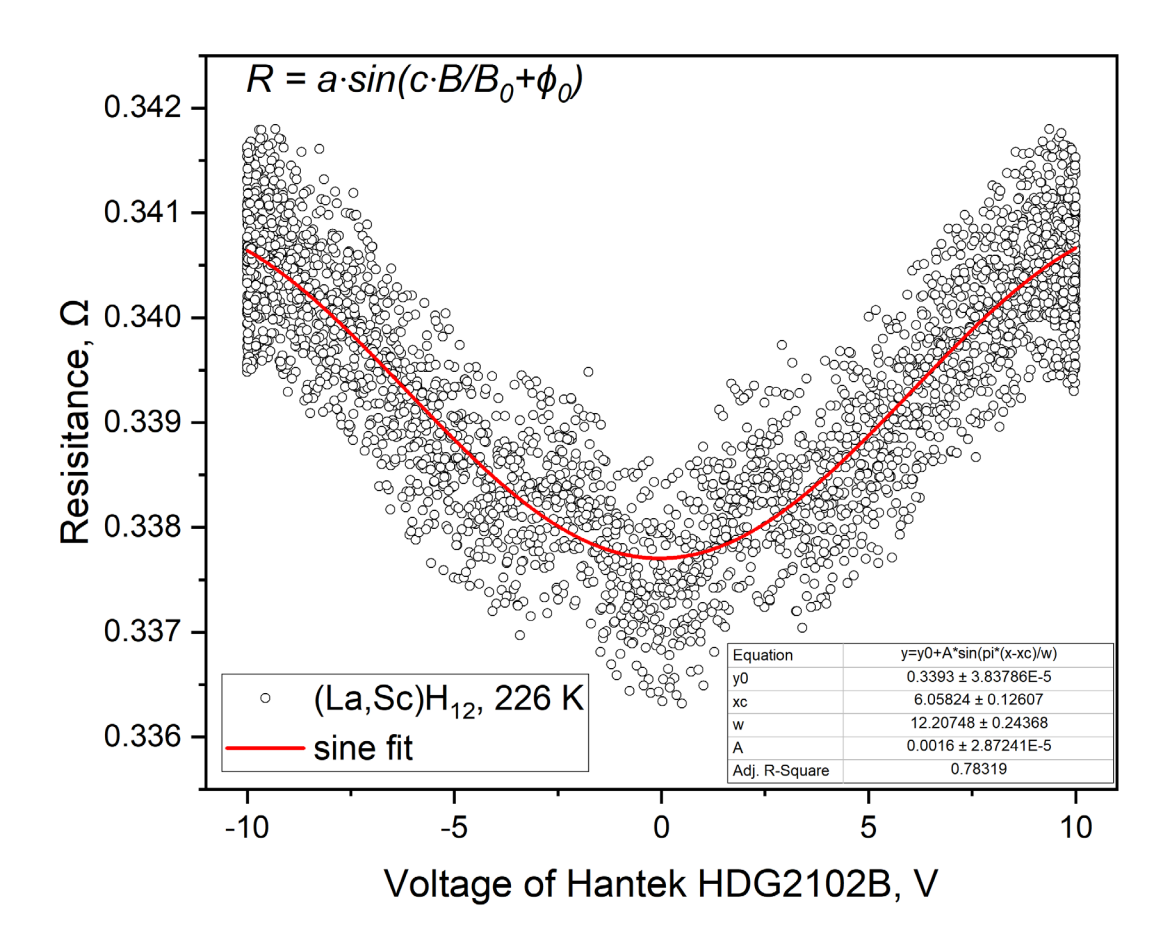


Figure S24. The dependence of the (La, Sc)H₁₂ sample (DAC LS-3) resistance on the voltage amplitude U_{max} on solenoid connected with the Hantek HDG2102B generator. The voltage of $U_{max} = 10$ V corresponds to the magnetic field of about ~ 10 G.

5. Theoretical calculations

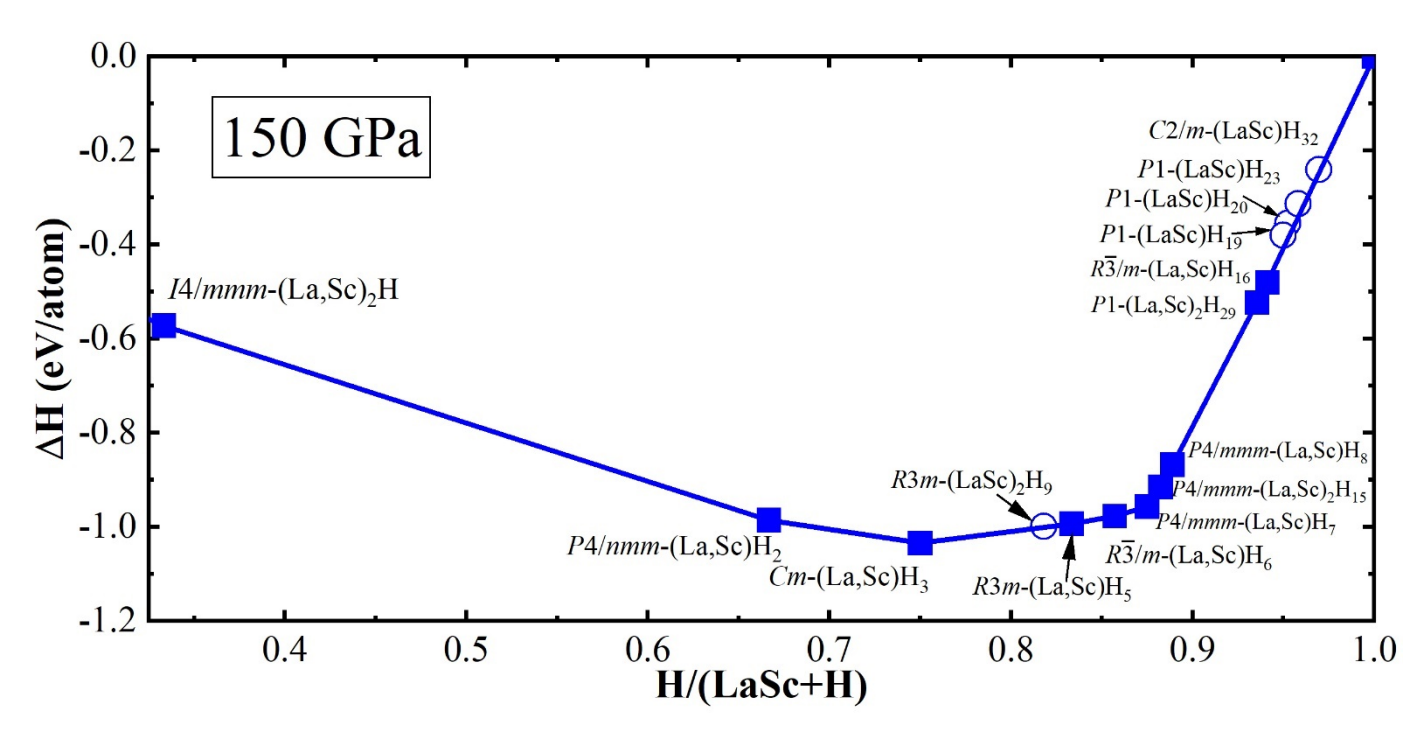


Figure S25. Convex hull of (LaSc)-H system at 150 GPa and 0 K calculated without accounting of zero-point energy effects in harmonic approximation.

Table S3. Results of an evolutionary search by USPEX 2023.0 code (python version) for stable structures in the (LaSc)-H system at 150 GPa and 0 K after 63 generations. All structures given in the Table lie on the convex hull.

ID	Origin	Formula	Enthalpy, eV	Volume, Å ³
597	Heredity	LaScH ₅	11.303	34.427
986	Permutation	LaScH ₁₆	3.342	54.236
1097	Heredity	$La_2Sc_2H_{15}$	16.348	78.703
1768	Permutation	$La_2Sc_2H_{29}$	8.371	101.814
1912	Heredity	LaScH ₇	8.562	38.935
2100	Permutation	LaSc	0.0	24.42
2504	Transmutation	$La_2Sc_2H_6$	28.34	62.246
3191	Transmutation	LaScH ₈	7.882	39.984
4203	Permutation	$La_2Sc_2H_1$	37.514	50.986
4997	Permutation	$La_2Sc_2H_4$	31.749	57.239
4998	Permutation	LaScH ₆	9.898	37.143
5075	RandSymPyXtal	H_{24}	-12.559	34.427

Table S4. Structures of the most thermodynamically stable (LaSc)-H phases found by USPEX at 150 GPa in the POSCARS format.

EA597	EA986
1.0000000000000000	1.0000000000000000
2.668835 -0.668172 0.097448	6.406570 -0.269267 -0.217726
-0.024904 5.475358 -0.032237	2.039868 2.870803 -0.448799
-1.337060 0.694375 2.307773	0.032796 -1.753643 3.087161
H La Sc	H La Sc
5 1 1	16 1 1
Direct	Direct
0.990937 0.659182 0.782584	0.612789 0.490501 0.015401
0.672738 0.731842 0.067006	0.112675 0.685290 0.867703
0.272191 0.580923 0.455271	0.416844 0.762801 0.656432
0.783584 0.083400 0.957256	0.938054 0.882364 0.957541
0.115508 0.075431 0.626459	0.242689 0.841667 0.929501
0.548628 0.363730 0.212518	0.794125 0.416004 0.223776

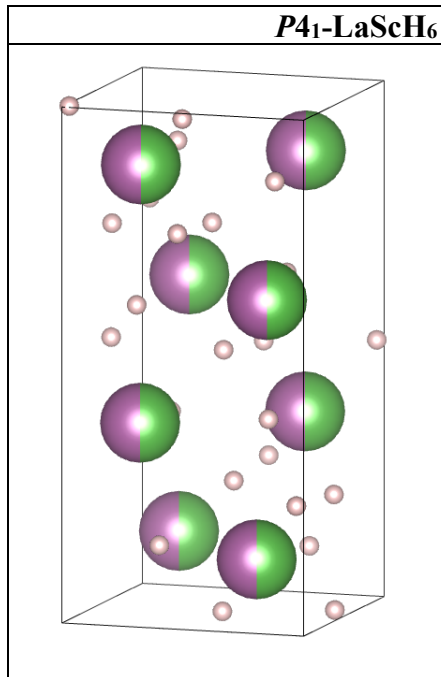
0.387589 0.888737 0.345047	0.419896 0.768684 0.144970
	0.236922 0.326543 0.396982
	0.796163 0.952893 0.770890
	0.247032 0.313620 0.944880 0.791696 0.936069 0.228844
	0.620017 0.479216 0.500999
	0.104169 0.348493 0.187743
	0.616608 0.992743 0.003717
	0.915610 0.590387 0.304904
	0.422345 0.254610 0.155043
	0.027939 0.109925 0.573076
	0.517152 0.127020 0.580492
EA1097	EA1768
1.0000000000000000	1.0000000000000000
5.171060 0.318179 0.233481	5.339820 0.343504 -0.002025
-0.251795 3.862650 0.164362	-0.241826 3.697004 0.009448
-0.166062 -0.178357 3.909404	0.036292 -0.037618 5.135654
H La Sc	H La Sc
15 2 2	29 2 2
Direct 0.671455 0.274826 0.511113	Direct 0.894097 0.916884 0.273566
0.071433 0.274826 0.311113 0.232132 0.032151 0.270222	0.894097 0.916884 0.273366 0.306533 0.931676 0.687301
0.232132 0.032131 0.270222 0.929148 0.766685 0.521268	0.629878 0.648803 0.634121
0.024183 0.289942 0.028582	0.719024 0.400374 0.111986
0.113852 0.782533 0.517027	0.689515 0.384030 0.766685
0.223255 0.533944 0.776385	0.630672 0.654462 0.254839
0.234524 0.523447 0.268910	0.443717 0.656674 0.320755
0.221042 0.023628 0.768052	0.286807 0.378016 0.181500
0.364815 0.280541 0.531332	0.886480 0.435410 0.259531
0.810726 0.528163 0.780820	0.955495 0.059363 0.546299
0.815171 0.518652 0.261781	0.970397 0.227924 0.330171
0.810063 0.030807 0.265478	0.447802 0.661873 0.569694
0.817913 0.036549 0.783093	0.182201 0.170516 0.557617
0.671058 0.791367 0.029314 0.367565 0.787910 0.015040	0.292554 0.941535 0.203397 0.954616 0.642036 0.761682
0.528139 0.785038 0.522824	0.602287 0.110880 0.023207
0.530794 0.292157 0.018947	0.768342 0.670118 0.446561
0.023808 0.772180 0.022473	0.974381 0.674893 0.125648
0.023163 0.276832 0.520719	0.830806 0.660590 0.940513
	0.156095 0.655371 0.061872
	0.887290 0.406893 0.622895
	0.396173 0.181033 0.790449
	0.674066 0.967878 0.774710
	0.433135 0.156824 0.038347
	0.317968 0.393120 0.687400
	0.216989 0.130386 0.297290
	0.728988 0.906350 0.107085
	0.158243 0.657832 0.815689
	0.877262 0.891329 0.626250 0.575652 0.152496 0.442838
	0.575052 0.152496 0.442838 0.020766 0.166374 0.930135
	0.486348 0.654871 0.942409
	0.110349 0.668510 0.444720
EA1912	EA2100
1.0000000000000000	1.0000000000000000000000000000000000000
5.590672 -1.319490 -0.510131	2.555205 0.603244 0.004092
0.645850 2.688712 0.139706	-0.813713 3.446689 0.002238
-1.096384 0.131270 2.542350	-0.003625 -0.002612 2.626398
H La Sc	La Sc
7 1 1	1 1
Direct	Direct
0.217875 0.540717 0.557568	0.282126 0.708674 0.069292
0.797993 0.536291 0.139413	0.783583 0.207064 0.558263
0.661208 0.537833 0.483743	
0.356208 0.509129 0.195337	
0.215553 0.011337 0.036547	

0.000500 0.031014 0.337335	
0.801129 0.035765 0.618422	
0.502434 0.027681 0.820827	
0.000837 0.535091 0.834229	F10101
EA2504	EA3191
1.000000000000000	1.0000000000000000
9.210557 -0.939627 1.352709 -0.182925 1.564494 2.258593	5.224338 0.100430 0.030453 -0.053569 2.761278 -0.133541
-0.182923 1.304494 2.238393 -0.240218 -2.766571 0.210050	-0.033369 2.761278 -0.133341 -0.022066 0.133248 2.764108
-0.240218 -2.700371 0.210030 H La Sc	-0.022000 0.133248 2.704108 H La Sc
6 2 2	8 1 1
Direct	Direct
0.890846 0.264615 0.102631	0.710620 0.577797 0.009334
0.291086 0.261590 0.100364	0.575794 0.082457 0.023771
0.165998 0.569621 0.767439	0.128153 0.073201 0.522578
0.043099 0.898563 0.435377	0.003103 0.605764 0.541516
0.352968 0.567262 0.731169	0.823821 0.589129 0.526580
0.097453 0.250710 0.114841	0.137460 0.595814 0.005531
0.502249 0.224749 0.043495	0.704791 0.094468 0.526948
0.739220 0.916087 0.390588	0.267766 0.077620 0.034066
0.984083 0.585298 0.786155	0.419898 0.583175 0.529256
0.233485 0.905222 0.429921	0.923803 0.095907 0.031336
EA4203	EA4997
1.0000000000000000	1.0000000000000000
3.607190 0.407292 0.091988 -2.220233 2.965481 2.805752	2.639027 -0.022500 0.022870 0.022260 2.638321 0.014768
0.031734 -1.043071 3.464114	0.012840 -0.077000 8.220089
H La Sc	H La Sc
1 2 2	4 2 2
Direct	Direct
0.139060 0.968623 0.936552	0.085919 0.625339 0.228064
0.872182 0.418519 0.208082	0.596937 0.122542 0.978242
0.430806 0.531492 0.646574	0.618507 0.613524 0.094750
0.651309 0.976957 0.924069	0.109137 0.116899 0.093650
0.137305 0.964030 0.434434	0.578777 0.098376 0.719039
	0.100260 0.615196 0.474928
	0.598488 0.103831 0.234713
T. 4000	0.107623 0.596112 0.958754
EA4998	EA5075
1.0000000000000000 5.700874 0.218452 0.389112	1.000000000000000 4.511691 -0.172302 0.009738
-0.037105 2.735489 -0.565684	-0.132127 3.291453 0.002085
-0.813919 -0.911795 2.506160	-0.009422 -0.002850 3.066034
H La Sc	H
6 1 1	24
Direct	Direct
0.023251 0.468701 0.613412	0.045833 0.788389 0.992944
0.459208 0.955897 0.605884	0.535071 0.290058 0.490189
0.194548 0.203850 0.080806	0.547251 0.301617 0.738417
0.546320 0.319912 0.300200	0.547805 0.781566 0.683748
0.624441 0.691859 0.057385	0.292671 0.008582 0.235425
0.106994 0.851443 0.379367	0.665927 0.944687 0.028332
0.828866 0.088113 0.829725	0.911600 0.639541 0.644892
0.328683 0.569186 0.825364	0.045776 0.278226 0.940151
	0.304839 0.536549 0.410459 0.795308 0.548264 0.266860
	0.795308 0.348264 0.266860 0.542723 0.775479 0.449776
	0.404089 0.132809 0.126182
	0.798749 0.046225 0.902294
	0.297091 0.043318 0.757675
	0.046324 0.291132 0.166917
	0.033820 0.769753 0.228049
	0.783606 0.534531 0.760339
	0.172486 0.442442 0.528858
	0.278923 0.511175 0.925941
	0.664539 0.454020 0.124699

Table S5. Calculated unit cell volume data used in this work to estimate the hydrogen content of synthesized La-Sc polyhydrides. Most of the calculations were done in Quantum ESPRESSO, with the exception of one calculation done using VASP code. The protypes used were I4/mmm-LaH₄ for (La, Sc)H₄, $Fm\overline{3}m$ -LaH₃ for (La, Sc)H₃, and $P6_3/mmc$ -ScH₆ for (La, Sc)H₆.

Compound	Pressure, GPa	Unit cell volume, Å ³ /(La,Sc)	Compound	Pressure, GPa	Unit cell volume, Å ³ /(La,Sc)
Tetragonal	30	29.17	sc-ScH ₁₂	200	28.7
(La,Sc)H ₄	150	20.09	<i>P</i> 6/ <i>mmm</i> - (La,Sc)H ₈	190	25.10
Cubic (La,Sc)H ₃	30	27.77	P6 ₃ /mmc- (La,Sc)H ₆	190	22.11 (VASP)
	150	19.32	Tetragonal (La,Sc)H ₄	190	18.72
P6 ₃ /mmc-	150	23.64	Cubic	200	17.69
$(La,Sc)H_6$			(La,Sc)H ₃	190	17.98

Table S6. Cif files of the most thermodynamically stable structures in the (LaSc)-H system found by USPEX code at 30 GPa.



 $\begin{array}{lll} La_4Sc_4H_{24} \\ Space \ Group: \ P\ 41 \ \ (\#76\text{-}1) \\ a = \ 4.78257 \ \mathring{A} & \alpha = 90.0000^\circ \\ b = \ 4.78257 \ \mathring{A} & \beta = 90.0000^\circ \\ c = \ 9.83966 \ \mathring{A} & \gamma = 90.0000^\circ \\ V = \ 225.0621 \ \mathring{A}^3 \end{array}$

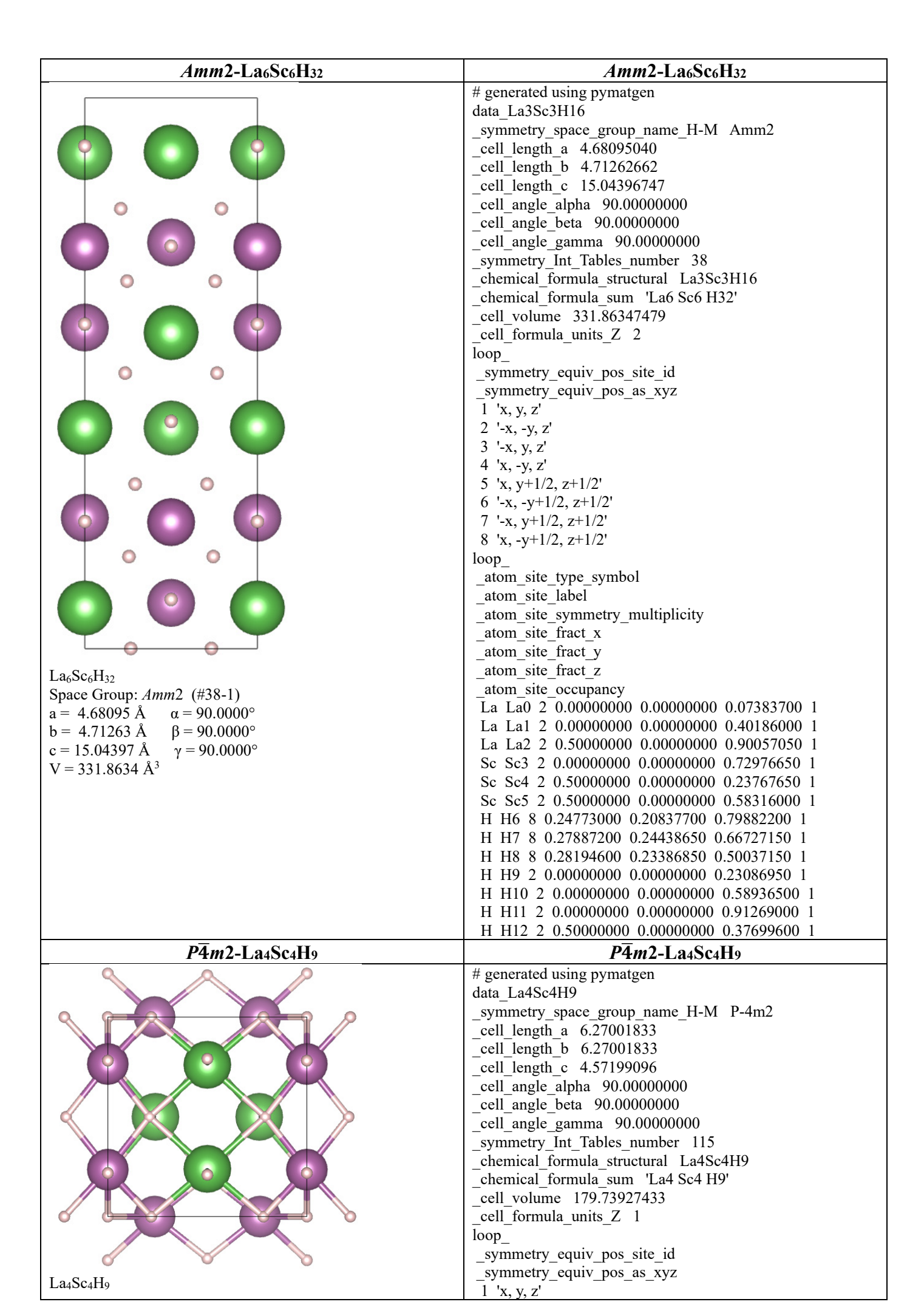
```
P41-LaScH6
# generated using pymatgen
data LaScH6
_symmetry_space_group_name_H-M P4 1
_cell_length_a 4.78256806
cell_length_b 4.78256806
cell length c 9.83965941
cell angle alpha 90.00000000
cell angle beta 90.00000000
cell angle gamma 90.00000000
_symmetry_Int_Tables number 76
chemical formula structural LaScH6
chemical formula sum 'La4 Sc4 H24'
cell volume 225.06210918
cell formula units Z 4
_symmetry_equiv_pos_site_id
symmetry equiv pos as xyz
1 'x, y, z'
2 '-y, x, z+1/4'
3'-x, -y, z+1/2'
4 'y, -x, z+3/4'
loop_
_atom_site_type_symbol
_atom_site_label
atom_site_symmetry_multiplicity
_atom_site_fract_x
atom site fract y
atom site fract z
atom site occupancy
La La0 4 0.23330400 0.75419200 0.87643200 0.5
 Sc Sc0 4 0.23330400 0.75419200 0.87643200 0.5
 La La1 4 0.23606500 0.27271500 0.62377100 0.5
 Sc Sc1 4 0.23606500 0.27271500 0.62377100 0.5
H H2 4 0.01839000 0.03586500 0.74979600 1
 H H3 4 0.02676200 0.53132800 0.26402200 1
H H4 4 0.03606600 0.51411700 0.48635500 1
 H H5 4 0.19942600 0.75731300 0.10734400 1
 H H6 4 0.25168400 0.68070100 0.63941600 1
H H7 4 0.45890000 0.48883200 0.50039600 1
```

Pm-La₃Sc₃H₁₆

 $\begin{array}{lll} La_3Sc_3H_{16} \\ Space \ Group: \ P\ m\ \ (\#6\mbox{-}1) \\ a=\ 4.69234\ \mathring{A} & \alpha=90.0000^\circ \\ b=\ 4.69614\ \mathring{A} & \beta=107.2486^\circ \\ c=\ 7.88047\ \mathring{A} & \gamma=90.0000^\circ \\ V=\ 165.8433\ \mathring{A}^3 \end{array}$

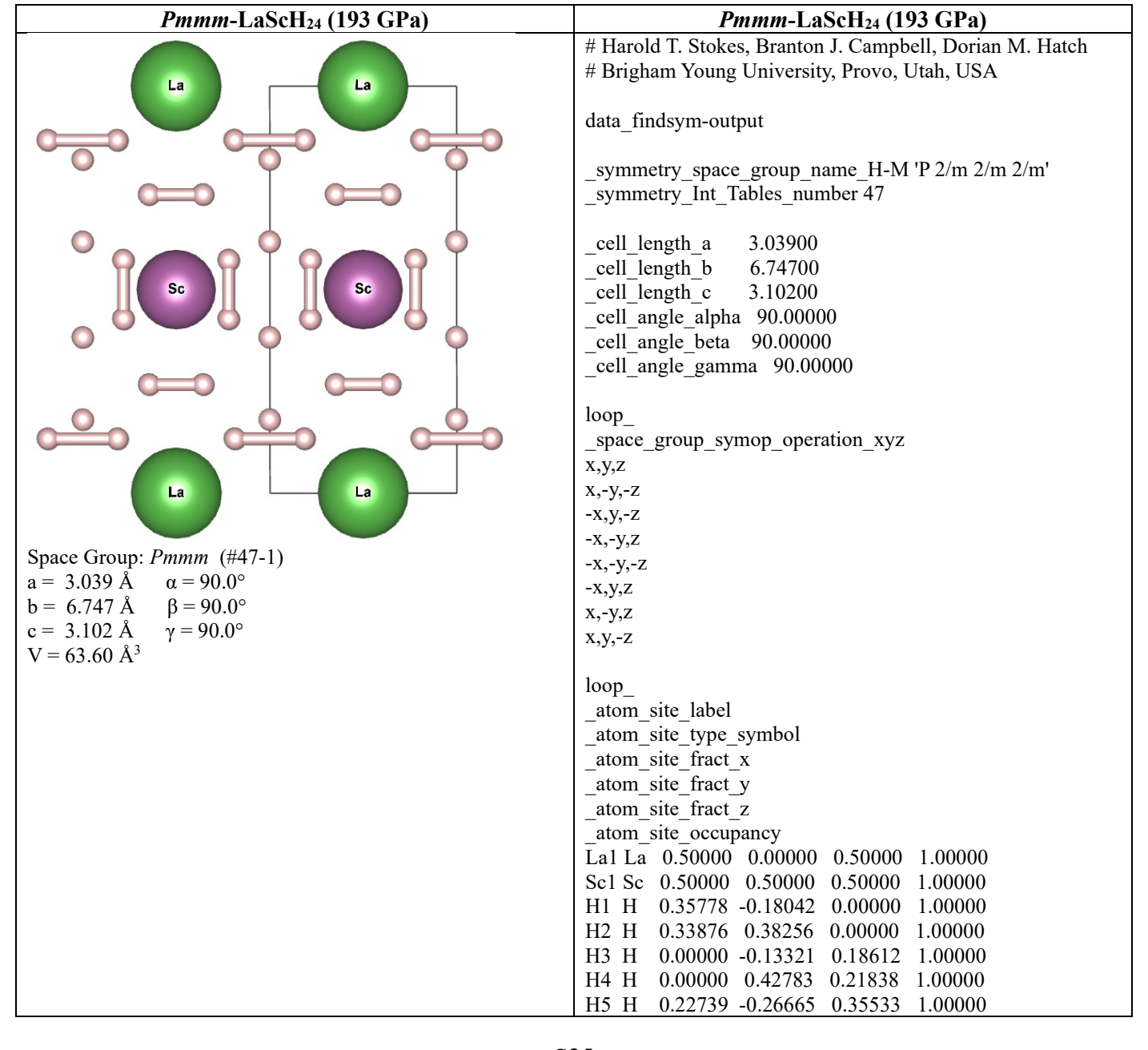
generated using pymatgen data La3Sc3H16 _symmetry_space_group_name_H-M Pm _cell_length_a 4.69234051 cell length b 4.69613509 cell length c 7.88046544 cell angle alpha 90.00000000 cell angle beta 107.24855117 cell angle gamma 90.00000000 symmetry Int Tables number 6 chemical formula structural La3Sc3H16 chemical formula sum 'La3 Sc3 H16' cell volume 165.84325821 cell formula units Z 1 loop symmetry_equiv_pos_site_id _symmetry_equiv_pos_as_xyz 1 'x, y, z' 2 'x, -y, z' loop_ _atom_site_type_symbol _atom_site_label _atom_site_symmetry_multiplicity atom site fract x _atom_site_fract_y atom site fract z atom site occupancy La La0 1 0.00646800 0.50000000 0.59943400 0.5 Sc Sc0 1 0.00646800 0.50000000 0.59943400 0.5 La La1 1 0.17363800 0.00000000 0.94586600 0.5 Sc Sc1 1 0.17363800 0.00000000 0.94586600 0.5 La La2 1 0.67075700 0.50000000 0.95585600 0.5 Sc Sc2 1 0.67075700 0.50000000 0.95585600 0.5 Sc Sc3 1 0.36523500 0.50000000 0.29901000 0.5 La La3 1 0.36523500 0.50000000 0.29901000 0.5 Sc Sc4 1 0.47918400 0.00000000 0.58538400 0.5 La La4 1 0.47918400 0.00000000 0.58538400 0.5 Sc Sc5 1 0.84141600 0.00000000 0.29007800 0.5 La La5 1 0.84141600 0.00000000 0.29007800 0.5 H H6 2 0.05047700 0.23141100 0.15154700 1 H H7 2 0.18608200 0.23378700 0.42756300 1 H H8 2 0.35597600 0.23723200 0.76350600 1 H H9 2 0.50531600 0.23190100 0.15811500 1 H H10 2 0.63692000 0.22710000 0.43301000 1 H H11 2 0.78160100 0.22297000 0.75653600 1 H H12 1 0.00785400 0.00000000 0.57813000 1 H H13 1 0.15429400 0.50000000 0.93470300 1 H H14 1 0.69459200 0.00000000 0.99877400 1 H H15 1 0.82041600 0.50000000 0.29216100 1

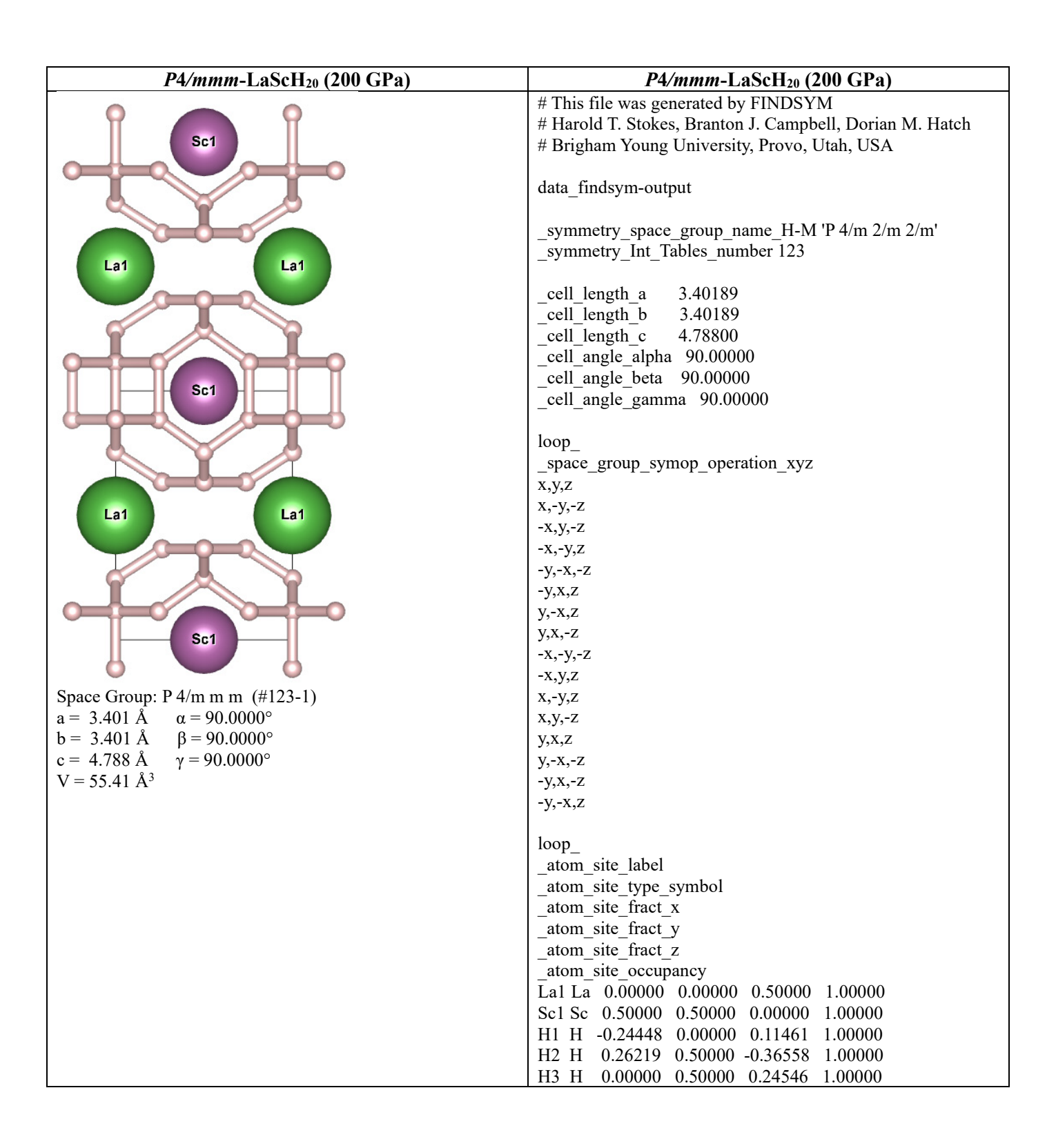
Pm-La₃Sc₃H₁₆



```
Space Group: P-4m2 (#115-1)
                                                                     'y, -x, -z'
a = 6.27002 \text{ Å} \alpha = 90.0000^{\circ}
                                                                   3 '-x, -y, z'
                  \beta = 90.0000^{\circ}
b = 6.27002 \text{ Å}
                                                                   4 '-y, x, -z'
                  \gamma = 90.0000^{\circ}
c = 4.57199 \text{ Å}
                                                                   5 '-x, y, z'
V = 179.7393 \text{ Å}^3
                                                                   6 '-y, -x, -z'
                                                                   7'x, -y, z'
                                                                   8 'y, x, -z'
                                                                  loop
                                                                  _atom_site_type_symbol
                                                                  atom site label
                                                                  atom site symmetry multiplicity
                                                                  _atom_site_fract_x
                                                                  atom site fract y
                                                                  _atom_site_fract_z
                                                                   atom site occupancy
                                                                   La La0 4 0.23929750 0.50000000 0.25605450 1
                                                                   Sc Sc1 4 0.00000000 0.23522250 0.75785650 1
                                                                   H H2 4 0.00000000 0.21842150 0.18872750 1
                                                                   H H3 4 0.20951850 0.50000000 0.74912250 1
                                                                   H H4 1 0.00000000 0.00000000 0.50000000 1
```

Table S7. Cif files of structures of La-Sc polyhydrides used in this work for superconductivity calculations. LaScH₂₄ is derivative of ScH₁₂ 24 , while LaScH₂₀ is derivative of canonical cubic LaH₁₀.





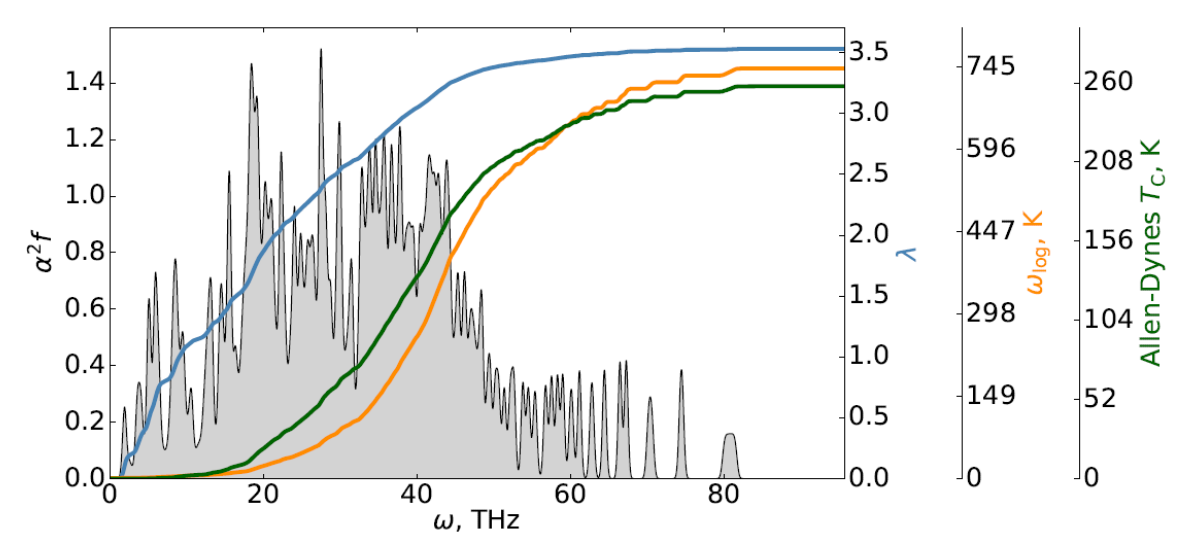


Figure S26. Eliashberg function, electron-phonon interaction parameter, logarithmically averaged frequency and critical temperature calculated using the Allen-Dean formula ²⁷ with $\mu^* = 0.1$ for the *Pmmm*-LaScH₂₄ structure at 193 GPa. The *q*-mesh density was $4 \times 4 \times 4$, and the *k*-mesh density was chosen to be $12 \times 12 \times 12$. To construct the graphs, we used the script proposed by G. Shutov ³⁶.

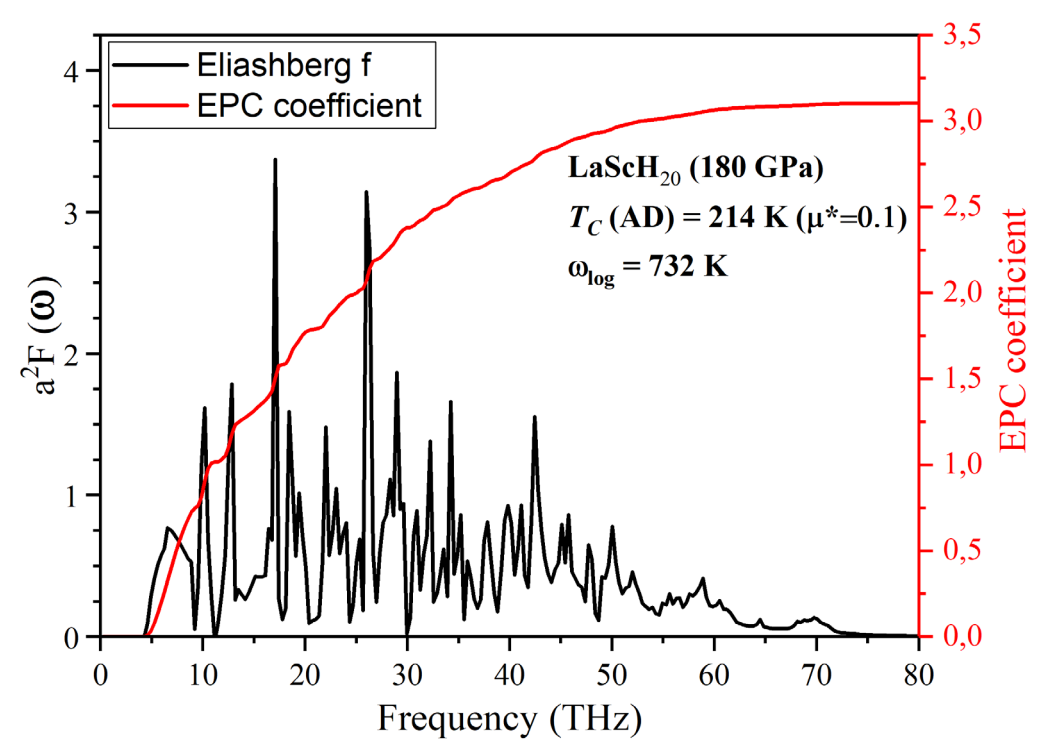


Figure S27. Eliashberg function, electron-phonon interaction parameter, logarithmically averaged frequency and critical temperature calculated using the Allen-Dean formula 27 with $\mu^* = 0.1$ for the P4/mmm-LaScH₂₀ structure at 180 GPa. The q-mesh density was 3 × 3 × 2, and the k-mesh density was chosen to be 12 × 12 × 12 for electronic wavefunctions and 18 × 18 for electron-phonon calculations.

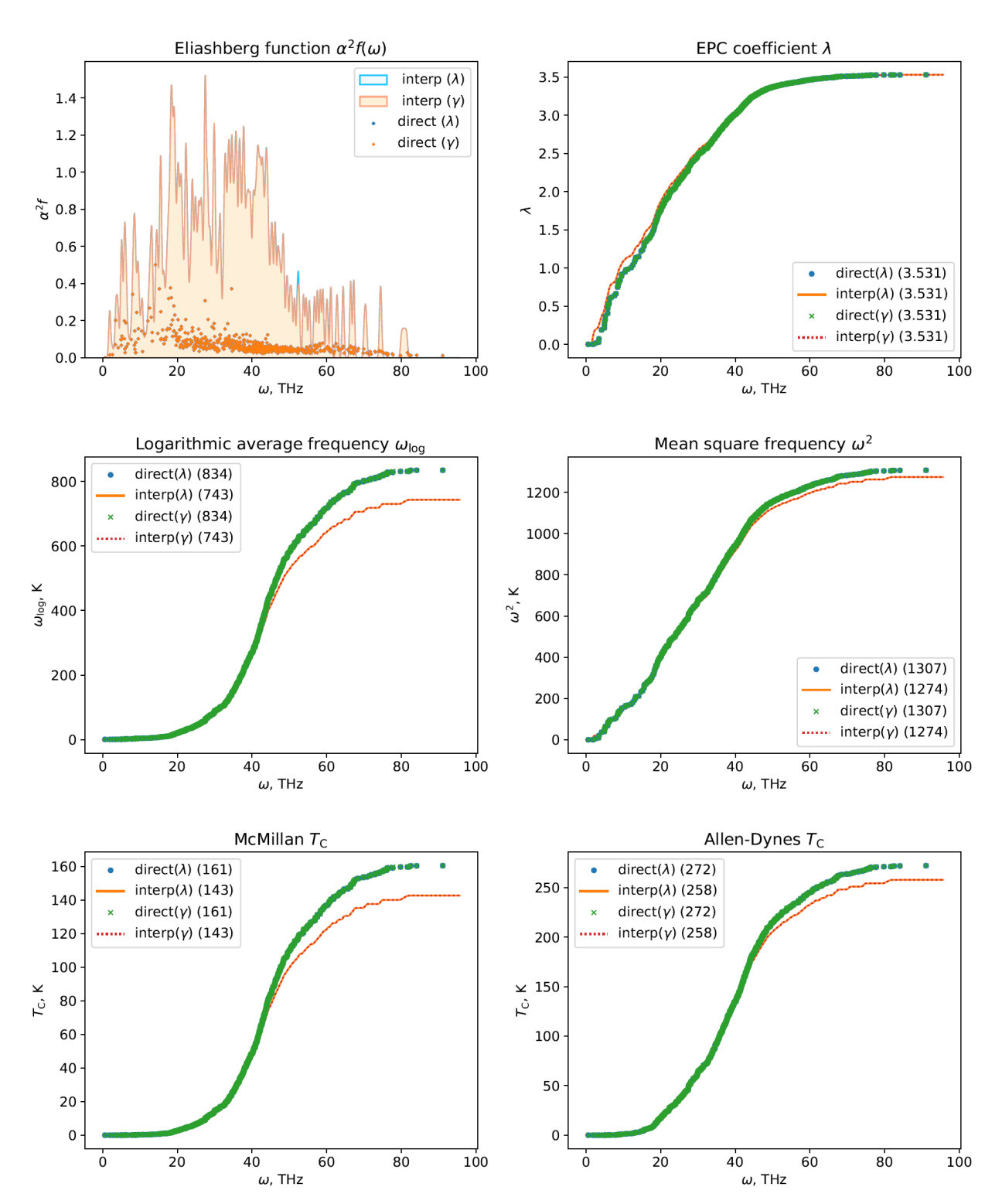


Figure S28. Convergence, Eliashberg and integral functions of frequency of various parameters of electron-phonon interaction in LaScH₂₄ at 193 GPa. Smoothing was used in the region ω = 0...3 THz. Coulomb pseudopotential is μ* = 0.1. To construct the graphs, a script written by G. Shutov ³⁶ was used. Results are as follows: λ=3.53, $ω_{log} = 743-834$ K, $ω_2 = 1274-1306$ K, calculated Allen-Dynes $T_c = 272$ K and the Eliashberg $T_c = 282$ K.

${\rm LaScH_{20}}$ Smoothing: 3 THz, resolution = 111, σ = 1, μ =0.1

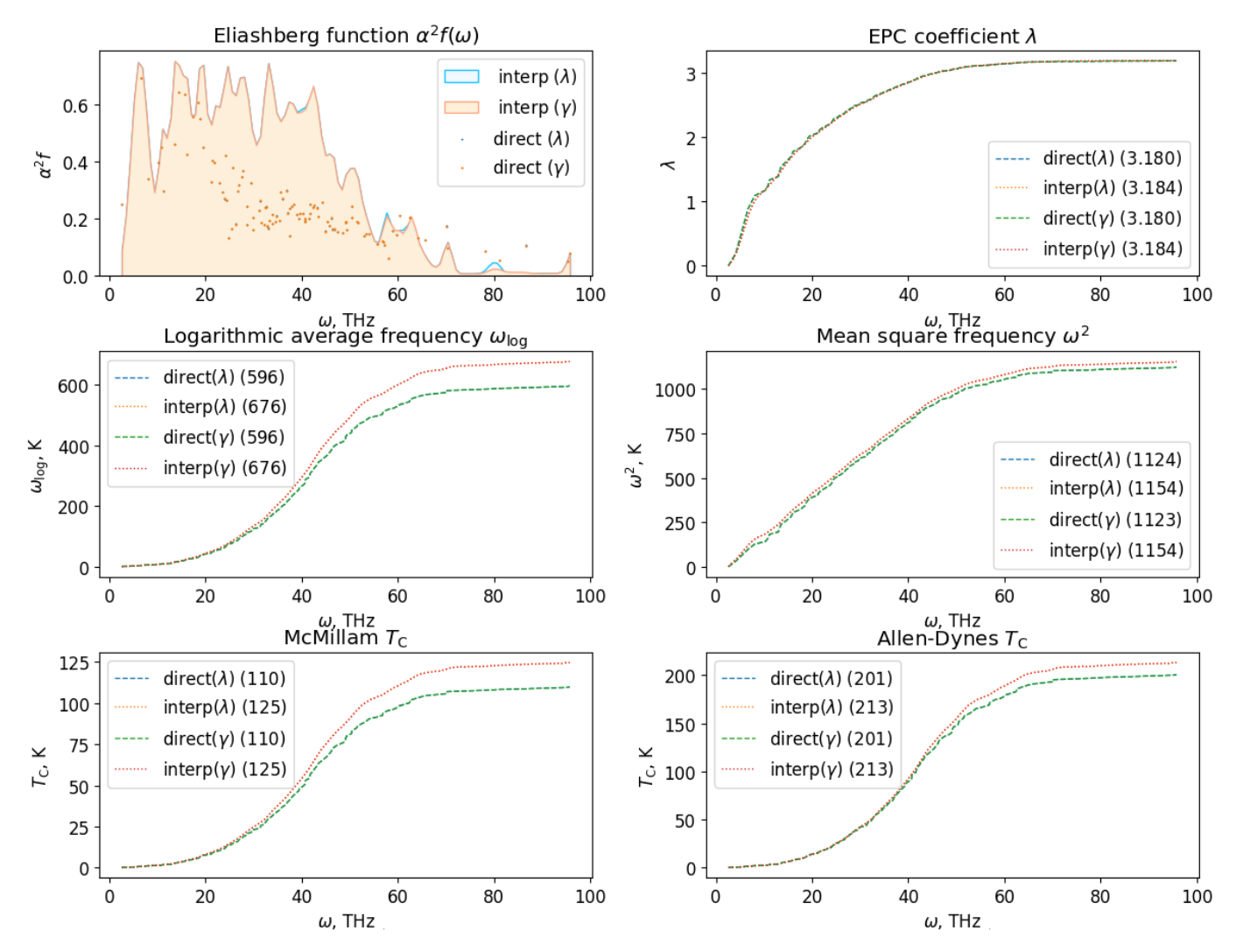


Figure S29. Convergence, Eliashberg and integral functions of frequency of various parameters of electron-phonon interaction in P4/mmm-La₂Sc₂H₄₀ at 200 GPa. Smoothing was used in the region $\omega = 0...3$ THz, Coulomb pseudopotential is $\mu^* = 0.1$. To construct the graphs, a script written by G. Shutov ³⁶ was used. Results are as follows: $\lambda = 3.18$, $\omega_{log} = 596-676$ K, $\omega_2 = 1123-1154$ K, calculated Allen-Dynes $T_c = 201$ K and the Eliashberg $T_c = 221$ K.

6. References

- Prescher, C. & Prakapenka, V. B. DIOPTAS: a program for reduction of two-dimensional X-ray diffraction data and data exploration. *High Pressure Res.* **35**, 223-230, (2015).
- 2 Macrae, C. F. *et al.* Mercury 4.0: from visualization to analysis, design and prediction. *J. Appl. Crystallogr.* **53**, 226-235, (2020).
- Petříček, V., Dušek, M. & Palatinus, L. Crystallographic Computing System JANA2006: General features. *Z. Kristallogr.* **229**, 345-352, (2014).
- 4 Le-Bail, A. Whole powder pattern decomposition methods and applications: A retrospection. *Powder Diffraction* **20**, 316-326, (2005).
- Hrubiak, R., Smith, J. S. & Shen, G. Multimode scanning X-ray diffraction microscopy for diamond anvil cell experiments. *Review of Scientific Instruments* **90**, 025109, (2019).
- Oganov, A. R. & Glass, C. W. Crystal structure prediction using ab initio evolutionary techniques: Principles and applications. *J. Chem. Phys.* **124**, 244704, (2006).
- Oganov, A. R., Lyakhov, R. O. & Valle, M. How Evolutionary Crystal Structure Prediction Worksand Why. *Acc. Chem. Res.* **44**, 227-237, (2011).
- 8 Lyakhov, A. O., Oganov, A. R., Stokes, H. T. & Zhu, Q. New developments in evolutionary structure prediction algorithm USPEX. *Comput. Phys. Commun.* **184**, 1172-1182, (2013).
- 9 Pickard, C. J. & Needs, R. J. Structures at high pressure from random searching. *physica status solidi* (b) **246**, 536-540, (2009).
- Bushlanov, P. V., Blatov, V. A. & Oganov, A. R. Topology-based crystal structure generator. *Comput. Phys. Commun.* **236**, 1-7, (2019).
- Hohenberg, P. & Kohn, W. Inhomogeneous Electron Gas. *Phys. Rev.* **136**, B864-B871, (1964).
- Kohn, W. & Sham, L. J. Self-Consistent Equations Including Exchange and Correlation Effects. *Phys. Rev.* **140**, A1133-A1138, (1965).
- Perdew, J. P., Burke, K. & Ernzerhof, M. Generalized Gradient Approximation Made Simple. *Phys. Rev. Lett.* 77, 3865-3868, (1996).
- Kresse, G. & Joubert, D. From ultrasoft pseudopotentials to the projector augmented-wave method. *Phys. Rev. B* **59**, 1758-1775, (1999).
- 15 Blöchl, P. E. Projector augmented-wave method. *Phys. Rev. B* **50**, 17953-17979, (1994).
- Kresse, G. & Furthmüller, J. Efficient iterative schemes for ab initio total-energy calculations using a plane-wave basis set. *Phys. Rev. B* **54**, 11169, (1996).
- Kresse, G. & Hafner, J. Ab initiomolecular-dynamics simulation of the liquid-metal–amorphous-semiconductor transition in germanium. *Phys. Rev. B* **49**, 14251-14269, (1994).
- 18 Kresse, G. & Hafner, J. Ab initio molecular dynamics for liquid metals. *Phys. Rev. B* **47**, 558-561, (1993).
- Troyan, I. A. *et al.* Non-Fermi-Liquid Behavior of Superconducting SnH₄. *Adv. Sci.* **2303622**, 1-10, (2023).
- Giannozzi, P. *et al.* QUANTUM ESPRESSO: a modular and open-source software project for quantum simulations of materials. *J. Phys.: Condens. Matter* **21**, 395502, (2009).
- Giannozzi, P. *et al.* Advanced capabilities for materials modelling with Quantum ESPRESSO. *J. Phys.: Condens. Matter* **29**, 465901, (2017).
- Baroni, S., Gironcoli, S. d., Corso, A. D. & Giannozzi, P. Phonons and related crystal properties from density-functional perturbation theory. *Rev. Mod. Phys.* **73**, 515-562, (2001).
- Kawamura, M., Gohda, Y. & Tsuneyuki, S. Improved tetrahedron method for the Brillouin-zone integration applicable to response functions. *Phys. Rev. B* **89**, 094515, (2014).
- Jiang, Q. *et al.* Prediction of Room-Temperature Superconductivity in Quasi atomic H₂-Type Hydrides at High Pressure *arXiv*: 2302.02621, (2023).
- Eliashberg, G. M. Interactions between electrons and lattice vibrations in a superconductor. *Sov. Phys. JETP* **11**, 696-709, (1960).
- Allen, P. & Dynes, R. A computer program for numerical solution of the Eliashberg equation to find *Tc. Technical Report* **7** TCM/4/1974, (1974).
- Allen, P. B. & Dynes, R. C. Transition temperature of strong-coupled superconductors reanalyzed. *Phys. Rev. B* **12**, 905-922, (1975).

- Baumgartner, T. *et al.* Effects of neutron irradiation on pinning force scaling in state-of-the-art Nb₃Sn wires. *Supercond. Sci. Technol.* **27**, 015005, (2013).
- Talantsev, E. F. & Tallon, J. L. Universal self-field critical current for thin-film superconductors. *Nat. Commun.* **6**, 7820, (2015).
- 30 BCS-theory-critical-current-fit (2023).
- 31 Semenok, D. *et al.* Evidence for Pseudogap Phase in Cerium Superhydrides: CeH₁₀ and CeH₉. *arXiv:2307.11742v2*, (2023).
- 32 Sadakov, A. V. *et al.* Vortex Phase Dynamics in Yttrium Superhydride YH₆ at Megabar Pressures. *J. Phys. Chem. Lett.* **14**, 6666-6671, (2023).
- Sadakov, A. V. *et al.* Quasi-two-dimensional vortex matter in the ThH₁₀ superhydride. *Phys. Rev. B* **109**, 224515, (2024).
- Guan, P.-W., Hemley Russell, J. & Viswanathan, V. Combining pressure and electrochemistry to synthesize superhydrides. *PNAS* **118**, e2110470118, (2021).
- He, X. *et al.* Predicted hot superconductivity in LaSc₂H₂₄ under pressure. *Proc. Natl. Acad. Sci.* **121**, e2401840121, (2024).
- 36 GitGreg228/a2f (2022).